TKK Dissertations 37
Espoo 2006

STABILITY DIAGNOSTICS FOR THIN-FILM PHOTOVOLTAIC MODULES

Doctoral Dissertation

Thomas Carlsson

Helsinki University of Technology
Department of Engineering Physics and Mathematics
Laboratory of Advanced Energy Systems

TKK Dissertations 37
Espoo 2006

STABILITY DIAGNOSTICS FOR THIN-FILM PHOTOVOLTAIC MODULES

Doctoral Dissertation

Thomas Carlsson

Dissertation for the degree of Doctor of Science in Technology to be presented with due permission of the Department of Engineering Physics and Mathematics for public examination and debate in Auditorium F1 at Helsinki University of Technology (Espoo, Finland) on the 22nd of September, 2006, at 12 noon.

Helsinki University of Technology
Department of Engineering Physics and Mathematics
Laboratory of Advanced Energy Systems

Teknillinen korkeakoulu
Teknillisen fysiikan ja matematiikan osasto
Energiatieteet

Distribution:
Helsinki University of Technology
Department of Engineering Physics and Mathematics
Laboratory of Advanced Energy Systems
P.O.Box 4100
FI - 02015 TKK
FINLAND
URL: http://www.tkk.fi/Units/AES/
Tel. +358-9-451 3198
Fax. +358-9-451 3195
E-mail: thomas.carlsson@tkk.fi

ISBN 951-22-8274-7
ISBN 951-22-8275-5 (PDF)
ISSN 1795-2239
ISSN 1795-4584 (PDF)
URL: http://lib.tkk.fi/Diss/2006/isbn9512282755/

TKK-DISS-2160

Otamedia Oy
Espoo 2006

Foreword

The doctoral work presented in this thesis was carried out between 2001 and 2005 at the Advanced Energy Systems laboratory at Helsinki University of Technology. It also included a research visit to Durham University, England.

Lifetime and stability research for photovoltaic modules is a multidisciplinary field with many different aspects and a lot of unexplored territory. Many research problems in this field require creative processing because no simple methods are available for solving them. This has been the most challenging and rewarding aspect of making this thesis. Looking back on the four years of work which are summarized here, it has been a very positive experience which has taught me much more than I initially expected. The field of photovoltaics is set for exciting developments and growth in the future, and I hope that this work can provide new ideas and questions for future studies.

I firstly want to thank my supervisor, professor Peter Lund, for giving me the opportunity to perform this work and for suggesting to me directions in which to proceed while giving me enough freedom to find my own way. Thanks are also due to Petri Konttinen for encouragement and reminders on the importance of details and to Janne Halme, Minna Toivola, Jaakko Saarinen, Antti Tolvanen and Kim Åström for helpful research ideas and collaboration. Our group of postgraduate students deserve thanks for creating a great working environment in which help for any problem is only one or two doors away. I also thank my supervisor in Durham, Andy Brinkman, for giving me valuable advice and a lot of his time.

Best of thanks and a lot of love to my son Mathias for his daily reminders that play, sleep and food is all you need to be happy and to my wife Sanna for teaching me a lot about life and providing much support. I also thank my parents for all the help they have given me throughout the years and for setting the example I am now trying to follow as a father. And finally, thanks to my sisters Emilia and Mikaela for many great childhood memories.

This work has been funded by the European Union, the Finnish National Technology Agency TEKES, Svenska Litteratursällskapet i Finland and Magnus Ehrnrooths stiftelse.

Espoo, May 2006

Thomas Carlsson

HELSINKI UNIVERSITY OF TECHNOLOGY
P. O. BOX 1000, FI-02015 TKK
http://www.tkk.fi

ABSTRACT OF DOCTORAL DISSERTATION

Author Thomas Carlsson

Name of the dissertation

Stability diagnostics for thin-film photovoltaic modules

Date of manuscript 19.1.2006 | Date of the dissertation 22.9.2006

☐ Monograph ☒ Article dissertation (summary + original articles)

Department Engineering Physics and Mathematics
Laboratory Advanced Energy Systems
Field of research Photovoltaics
Opponent(s) Dr Hanne Lauritzen
Supervisor Professor Peter Lund

Abstract

Photovoltaic (PV) modules create electricity from solar radiation by converting photon energy to electrical potential energy. The use of photovoltaic electricity is growing rapidly particularly in building-integrated, grid-connected applications. The useful lifetime of PV modules is an important determinant of the competitiveness of PV electricity. Lifetime improvement and prediction requires detailed information on degradation mechanisms in the field and in accelerated aging tests. In this thesis, new methods for studying and predicting the stability of thin-film PV modules have been developed. Stability is a greater challenge for thin-film devices than for established PV technologies, and good stability diagnostics are therefore crucial for improvements in thin-film device lifetime.

The diagnostics developed in this thesis focused on two areas of lifetime research. The first was the study of water transport in photovoltaic module encapsulants. It was shown that a TiO_2 film of micrometer thickness can be used as a sensor structure to measure water transport in the encapsulant with high accuracy without affecting the transport process. The sensor concept was applied in a study of absorption and desorption of water in ethylene-vinyl-acetate (EVA) films laminated between two glass sheets. The rate of desorption at a temperature difference of 25°C between the sample and the surroundings was 16 times higher than the rate of absorption at ambient temperature. This result indicates that unframed, EVA-encapsulated modules are likely to dry out in sunny conditions.

The degradation of thin-film modules in outdoor operation was the second area of interest in this thesis. A de-encapsulation method for characterizing field degradation in thin-film modules was presented and applied to CdTe modules. It was observed that small-area sampling is especially well suited for characterizing module fill factor degradation. A data filtering methodology was also developed to improve the accuracy of data analysis in field tests. The method was applied to CIGS modules and was found to be especially useful in the analysis of low-irradiance data and current parameters. Additionally, thermal modeling of building integrated a-Si modules was used to predict thermal stress in different European locations.

The diagnostics developed in this thesis open up possibilities for improving thin-film module lifetime by enabling precise testing of the moisture-protection properties of encapsulants and by providing methods for identifying degradation mechanisms in field-tested modules.

Keywords photovoltaics, thin-film, stability, lifetime, encapsulation, field test

ISBN (printed) 951-22-8274-7 | ISSN (printed) 1795-2239

ISBN (pdf) 951-22-8275-5 | ISSN (pdf) 1795-4584

Number of pages 59 (summary) + 69 (articles)

Publisher Helsinki University of Technology

Print distribution Laboratory of Advanced Energy Systems

☒ The dissertation can be read at http://lib.tkk.fi/Diss/2006/isbn9512282755

TEKNISKA HÖGSKOLAN
PB 1000, FI-02015 TKK
http://www.tkk.fi

SAMMANFATTNING
AV DOKTORSAVHANDLING

Författare Thomas Carlsson

Titel

Stabilitetsdiagnostik för tunnfilmssolpaneler

Inlämningsdatum för manuskript 19.1.2006
Datum för disputation 22.9.2006

☐ Monografi ☒ Sammanläggningsavhandling (sammandrag + separata publikationer)

Avdelning Teknisk Fysik och Matematik
Laboratorie Energivetenskaper
Forskningsområde Solelektricitet
Opponent Dr Hanne Lauritzen
Övervakare Professor Peter Lund

Sammanfattning

Solpaneler producerar elektricitet genom att konvertera solljusets energi till elektrisk potentiell energi. Den globala marknaden för solelektricitet har vuxit betydligt under de senaste åren, speciellt inom system kopplade till elnätet. Ett sätt att förbättra solelektricitetens konkurrenskraft är att förlänga panelernas livslängd. Livslängdsförbättringar kräver detaljerad information om de mekanismer som försämrar solpanelers prestanda i olika förhållanden. I detta arbete har nya metoder utvecklats för undersökning och förutsägelser av tunnfilmssolpanelers stabilitet. Stabilitetsfrågorna är svårare att lösa för tunnfilmspaneler än för de mera etablerade solelteknologierna. Det är därför ytterst viktigt att dessa frågor kan studeras med effektiv stabilitetsdiagnostik.

Diagnostiken i denna avhandling har koncentrerats på två områden inom stabilitetsforskning. Det första var studier av vattentransport i solpanelers inkapslingsmaterial. Det visades att en TiO_2 film med några mikrometers tjocklek kan användas som en sensor för att med god precision karakterisera vattendiffusionsprocesser i inkapslingspolymerer. Sensorn tillämpades i en studie av vattenabsorption och -desorption i laminerade glas/etylen-vinyl-acetat(EVA)/glas prover. Då temperaturskillnaden mellan provet och omgivningen var ca 25^{o}C var desorptionshastigheten 16 gånger högre än absorptionshastigheten utan temperaturskillnad. Detta resultat antyder att paneler laminerade med EVA utan extra försegling troligen torkar betydligt i soliga förhållanden.

Den andra tyngdpunkten i denna avhandling var på studier av prestationsförmåga i fälttester. Tydliga försämringar i CdTe tunnfilmspanelers effekt studerades genom att inkapslingen öppnades och små prover tagna från panelerna analyserades. Provanalysen lämpade sig speciellt väl för studier av försämrad fyllnadsfaktor. I en annan del av arbetet utvecklades en metod för att förbättra fältresultatens analysering genom kontrollerad filtrering av mätdata. Metoden tillämpades på CIGS tunnfilmspaneler, och den visade sig vara speciellt användbar för strömstorheter samt för all data som mätts vid låg strålningsintensitet. I denna avhandling modellerades också fasadintegrerade a-Si solpanelers termiska beteende för att uppskatta de termiska påfrestningarna på panelerna i olika europeiska klimat.

Diagnostiken som utvecklats i detta arbete kan användas till att förbättra tunnfilmssolpanelers livslängd. Den möjliggör detaljerade tester av fuktskyddet hos olika inkapslingssalternativ samt förbättrar den information som kan fås från fälttestade tunnfilmssolpaneler.

Ämnesord solelektricitet, tunnfilm, stabilitet, livstid, inkapsling, fälttest

ISBN (tryckt) 951-22-8274-7
ISSN (tryckt) 1795-2239
ISBN (pdf) 951-22-8275-5
ISSN (pdf) 1795-4584
Sidantal 59 (sammandrag) + 69 (publikationer)

Utgivare Tekniska Högskolan

Distribution av tryckt avhandling Laboratoriet för Energivetenskaper

☒ Avhandlingen är tillgänglig på nätet http://lib.tkk.fi/Diss/2006/isbn9512282755

Table of Contents

List of Publications

This thesis is an introduction to the following publications:

I. T.Carlsson, J.Halme, P.Lund, P.Konttinen.
'*Moisture sensor at glass/polymer interface for monitoring of photovoltaic module encapsulants*'
Sensors and Actuators A 125 (2006) p. 281-287.

II. T.Carlsson, P.Konttinen, P.Lund.
'*Absorption and desorption of water in glass/ethylene-vinyl-acetate/glass laminates*'
Polymer Testing, 2006, in press.

III. T.Carlsson, A.Brinkman.
'*Identification of Degradation Mechanisms in Field-tested CdTe Modules*'
Progress in Photovoltaics 14 (2006) p. 213-224.

IV. T.Carlsson, K.Åström, P.Konttinen, P.Lund.
'*Data Filtering Methods for Determining Performance Parameters in Photovoltaic Module Field Tests*'
Progress in Photovoltaics 14 (2006) p. 329-340.

V. P.Konttinen, T.Carlsson, P.Lund, T.Lehtinen.
'*Estimating Thermal Stress in BIPV Modules*'
International Journal of Energy Research, 2006, in press.

VI. H.-D.Mohring, D.Stellbogen, R.Schäffler, S.Oelting, R.Gegenwart, P.Konttinen, T.Carlsson, M.Cendagorta, W.Herrmann.
'*Outdoor Performance of Polycrystalline Thin Film PV Modules in Different European Climates*'
Proceedings of the 19th European Photovoltaic Solar Energy Conference, 2004, p. 2098-2101.

Summary of Publications and Author Contribution

I. A moisture sensor at the interface between a glass substrate and a polymer encapsulant was developed. A transparent conducting coating on the glass surface was patterned and used to measure the impedance of a TiO_2 film of micrometer thickness. The ac-resistance of the film depended approximately exponentially on water concentration in the film both when the film was open to the environment and when it was laminated under an ethylene-vinyl-acetate encapsulant. Implications of the calibration experiments for sensor usage in PV module encapsulant studies were discussed.

The moisture sensor concept was developed by the author in cooperation with the co-authors. Experiments were planned and conducted by the author. The author wrote the majority of the publication.

II. The moisture sensor developed in Publication I was used to measure the rate of water absorption and desorption inside glass/ethylene-vinyl-acetate/glass laminates at different temperatures. The absorption rate at room temperature was compared to the desorption rates when sample temperatures were higher than the temperature of the surroundings. The chosen temperatures corresponded approximately to conditions in the field. It was observed that a temperature difference slightly over 10^oC between sample and surroundings resulted in a 4 times higher desorption rate than the absorption rate in ambient conditions, and that a difference of 25^oC resulted in 16 times faster desorption than ambient absorption. The implications of these results on the moisture protection of PV modules were discussed.

The possibility of applying the sensor to absorption/desorption measurements was recognized by the author. Experiments were planned in cooperation with the co-authors and conducted by the author. The author wrote the publication.

III. Samples were taken from full-size CdTe PV modules whose performance had degraded significantly during field testing at Espoo, Finland. They were studied to uncover the degradation mechanisms responsible for module failure. Interconnect and cell failure mechanisms were separated from each other. Results indicated that decreased dopant concentration close to the junction and increased series resistance in the transparent front contact contributed to module failure in the field. The restrictions of small-area sampling in studies of large-area module degradation were presented in detail.

The author had an active role in the setup and maintenance of the field test measurements. Small sample analysis was planned and conducted by the author. Results were interpreted in cooperation with the co-author. The author wrote the publication.

IV. A methodology for improving analysis accuracy in PV module field testing was developed based on field test measurements of CIGS modules in Espoo, Finland. By filtering performance data with specific restrictions on key meteorological and module variables, changes in performance parameters could be monitored with 70–80% less data scattering than in standard analyses. A general methodology for choosing between different combinations of filtering criteria was developed and applied to the studied CIGS modules.

The author had an active role in the setup and maintenance of the field test measurements. The author developed the filter evaluation method and participated in the development of the temperature correction calculation. The author wrote the publication.

V. Thermal modeling of a building-integrated photovoltaic facade with amorphous silicon modules deployed in Espoo, Finland, and temperature measurements from the same facade were used to estimate the thermal stress which the modules would be exposed to in other European climates. This method of estimating thermal stress required only meteorological data from the location in question. The thermal stress was found to be more than 50% higher in Lisbon, Portugal, than in Espoo. Factors affecting estimation of thermal stress were discussed.

The author had an active part in planning and conducting the data analysis. The author participated in the thermal modeling of the facade and in the writing of the publication.

VI. Field tests of full-size CdTe and CIS photovoltaic modules were carried out in Finland, Germany and Spain. This paper describes the measurement methodology and test site characteristics of these field tests and presents the changes in basic performance parameters as a function of time, as well as their dependence on temperature and irradiance.

The author had an active role in the setup and maintenance of the field test measurements in Finland.

Nomenclature

A	Solar cell/module area (m^2)
C	Water concentration in EVA (mg/mm^3)
C_A	Constant in Arrhenius equation
C_{sat}	Saturation water concentration in EVA (mg/mm^3)
c	Water concentration in TiO_2 film (mg/mm3)
D	Diffusion coefficient of water in EVA (mm^2/s)
D_{back}	Degradation mode: back contact resistance
D_{cell}	Degradation mode: cell degradation
D_{SH}	Degradation mode: interconnect shunt resistance
D_{TCO}	Degradation mode: front contact resistance
$D_{TCO/back}$	Degradation mode: interconnect series resistance
E_a	Activation energy (eV)
f	Proportion of days with measurement data, a function of Ω (–)
G	Solar irradiance in module plane (W/m^2)
G_D	Diffuse horizontal irradiance (W/m^2)
G_H	Global horizontal irradiance (W/m^2)
G_0	Filtering criterion: solar irradiance in module plane (W/m^2)
I	Solar cell current (A or A/cm^2)
I_{MPP}	Maximum power point current (A or A/cm^2)
I_{SC}	Short-circuit current (A or A/cm^2)
J_0	Water flux in encapsulated sensor calibration ($mg/mm^2 \cdot s$)
k	Rate in Arrhenius equation
k_B	Boltzmann's constant ($1.38 \cdot 10^{-23}$ J/K)
L	EVA thickness (mm)
P_{MPP}	Maximum power (W or mW/cm^2)
R	G_H/G_D ratio (–)
R_{sensor}	Sensor ac-resistance (Ω)
R_{min}	Filtering criterion: G_H/G_D ratio (–)
R_S	Series resistance (Ω)
R_{SH}	Shunt resistance (Ω)
R_0	Reference ac-resistance for sensor (Ω)
r	Scaled resistance variable (–)
s	Sensor thickness (μm)
T	Temperature (K)
T_A	Accelerated aging temperature (K)
T_{amb}	Ambient temperature (K)
T_i	Indexed module temperature (K)
T_{max}	Filtering criterion: maximum module temperature (K)
T_{min}	Filtering criterion: minimum module temperature (K)
T_{mod}	Module temperature (K)
t	time (s)
V	Solar cell/module voltage (V)
V_{MPP}	Maximum power point voltage (V)
V_{OC}	Open circuit voltage (V)
x	Coordinate in encapsulated sensor calibration experiment
Y	Performance parameter of PV module
ΔG	Filtering criterion: width of plane-of-array irradiance interval (W/m^2)
Ω	Combination of data filtering criteria (–)

γ_i	Fraction of year spent at temperature T_i (–)
η	Efficiency (–)
θ	Angle of incidence of sunlight on PV module (^{o})
θ_{max}	Filtering criterion: maximum angle of incidence of sunlight (^{o})
θ_{min}	Filtering criterion: minimum angle of incidence of sunlight (^{o})
$\overline{\sigma_Y}$	Standard deviation in Y, a function of Ω (–)
τ_A	Module lifetime in accelerated aging test (h)
τ_N	Module lifetime in real operating conditions (h)

Abbreviations

a-Si	Amorphous silicon
BIPV	Building-integrated PV
CIS,CIGS	$Cu(In,Ga)Se_2$
c-Si	Crystalline silicon
EVA	Ethylene vinyl acetate
FF	Fill factor
ITO	Indium tin oxide
mc-Si	Multicrystalline silicon
NREL	National Renewable Energy Laboratory
PV	Photovoltaics
RH	Relative humidity
TCO	Transparent conducting oxide
WVTR	Water vapor transmission rate

1. Introduction

1.1. Photovoltaics in a wider perspective

Global energy usage is likely to be significantly transformed in the 21st century both in terms of energy sources and in terms of its effects on other aspects of society. World population is projected to increase from 6.5 billion in 2005 to 9.1 billion in 2050 [1] and energy consumption is predicted to be more than 50% higher in 2030 than it is today. A large part of this growth will take place in developing countries, where the lifestyles of hundreds of millions of people will be changed [2]. At the same time the age of fossil fuels will be ending as resources become scarce, so a transition to a very different energy economy will eventually take place. Adapting to the climatic consequences of past and present fossil fuel usage may be an even greater challenge than the technological transition. The production and consumption of energy, as well as its political and environmental consequences, will therefore remain an important issue on the global agenda.

When possible answers to the energy challenges of the coming century are compared, the long-term benefits of *renewable energy* are substantial. Renewable energy resources are inexhaustible. Most of them, including solar energy, wind energy, hydroelectric power and bioenergy, are driven by the absorption of sunlight in Earth's ecosystem. The guaranteed availability of renewable energy resources and their environmentally benign character are significant advantages over other solutions. However, at the present time renewable energy sources occupy fairly small segments of the energy market in most countries. Key reasons for this are that established energy sources are still being subsidized (worldwide subsidies for fossil fuels and nuclear energy were estimated at $145 billion per year in 1998 [3]) and that the infrastructure of modern society has been built around the established resources. On the other hand, positive developments such as deregulation of energy markets, new technological solutions and favorable public opinion offer hope that the renewable revolution in the energy sector is gradually coming closer.

The conversion of sunlight to electricity with photovoltaic (PV) systems is a renewable energy concept with promising future prospects. The total amount of radiative solar power striking Earth's surface exceeds the present-day energy consumption of mankind by a factor of about 15000. With PV modules the solar energy flux can be converted to electricity immediately without any harmful emissions. The solar energy resource is renewable, abundant and freely available across the globe. As an energy resource it differs significantly from fossil and nuclear fuels in that its availability does not depend on ownership and global commerce. Widespread utilization of solar energy would therefore provide a better basis for economic development in many poor regions of the world than the present energy system.

Solar electricity usage has been growing rapidly during the past decade, as exemplified by the increase in total PV system capacity from 110 MW in 1992 to 2596 MW in 2004 in countries participating in the IEA-PVPS programme [4]. This growth has occurred mainly in the field of PV systems connected to the electricity grid, which have surpassed stand-alone PV systems in cumulative installed capacity. Effective market subsidy programs in Japan and Germany have promoted the use of PV electricity both

in residential and public installations, proving that solar electricity can be a useful source of energy even at mid-latitudes. At the present time the price of PV electricity is estimated to be 0.6 €/kWh at locations with 900 sunshine hours per year and 0.3 €/kWh with 1800 sunshine hours. The peak price of conventional grid electricity is in the range 0.1 – 0.2 €/kWh, while the bulk price is usually below 0.05 € / kWh. In a recent European PV industry roadmap, it was projected that photovoltaics can provide competitive peak electricity in Southern European climates by 2010 and competitive bulk electricity by 2030 [5]. Cost reduction is the most important challenge for photovoltaic energy.

The price (expressed in €/W) and lifetime of the PV module are the most important factors determining PV electricity price (expressed in €/kWh). Module price can be reduced by increasing efficiency or producing the module more cheaply. Thin-film photovoltaic technologies represent a technological development with significant potential for cost reduction through more economic production processes. However, it is crucial that production benefits are not gained at the expense of other price factors. A fundamental challenge for thin-film PV technologies is to be competitive also in efficiency and lifetime in order benefit fully from their manufacturing advantage. Both performance and stability issues in thin-film photovoltaics involve difficulties which are not found in the established crystalline silicon PV technologies. The focus of this thesis is on the stability of thin-film PV modules, in particular on methods for studying and predicting module degradation.

1.2. Background and motivation for this study

PV module production costs, conversion efficiency and lifetime are all interdependent since performance and lifetime can be improved if higher costs are accepted, and maximizing performance in many cases requires special device designs which may not be durable. The lifetime of a module has a direct impact on the total amount of energy it will produce, which is a determinant of PV electricity price. For most PV technologies, stability questions have been given less research attention than production and performance issues. Lifetime improvement therefore provides ample scope for increasing the competitiveness of PV electricity.

Accurate evaluation of PV module lifetimes is crucial for estimating performance and issuing warranties. These can be used to estimate the return of an investment in PV electricity, where the initial investment usually is much larger than the operating costs. Testing modules in the field to study their stability in real operating conditions is a necessary requirement for reliable lifetime estimation. However, it is not practical to use only field testing, since lifetimes of at least 20 – 30 years are required today. Accelerated aging tests have to be used as a complement to test the stability of modules quickly and improve their design if problems are detected. Quick feedback cycles are especially crucial for thin-film photovoltaic technologies, which often exhibit significant variations in stability and performance properties between differently manufactured modules.

Accelerated aging tests are conducted in the laboratory by applying *stress factors* such as high temperature, temperature cycles, humidity and UV-light to the modules. The

three key tasks in estimating PV module lifetimes are the following: 1) the degradation mechanisms responsible for performance loss in the field should be identified, 2) it should be ensured that accelerated aging produces the right degradation mechanisms in the modules without introducing additional, unwanted degradation, and 3) it should be established how field lifetime can be calculated from accelerated aging test results [6].

It is evident that the most important issues in lifetime prediction are identification of degradation mechanisms and understanding of their dependence on stress factors. The aim of this thesis is to develop new diagnostic methods for studying degradation mechanisms which are relevant to thin-film PV technologies. The focus of the thesis is twofold: the first part deals with testing of encapsulant materials, in particular their moisture-protection properties which are known to be an important determinant of module lifetime [7]. A moisture sensor has been developed for measuring water concentration in encapsulated PV modules or laminated test samples. The sensor allows characterization of water diffusion processes in PV module encapsulants and detailed studies of the effect of polymer aging on water penetration.

The second topic of this thesis is field testing of thin-film modules, where the main focus is on identification of degradation mechanisms under real operating conditions. This is a difficult issue since a convenient duration for a field test sequence is about 4–5 years, even shorter if improved module designs are to be developed and tested based on the results. Consequently, changes in performance are small and difficult to detect. This thesis describes a method for de-encapsulation of field-tested thin-film modules which allows electrical characterization of samples from the module. A statistical methodology for improving the accuracy of PV module performance monitoring in field tests is also presented.

1.3. Outline of thesis

This thesis is divided into six chapters. This introduction is the first chapter. Chapter 2 presents the operating principles of solar cells, as well as the basics of thin-film photovoltaic technology. In Chapter 3 a literature review on the stability of thin-film PV modules is presented and the present status of stability research is discussed. Chapter 4 contains an introduction to the development of the moisture sensor and an application of the sensor to measurement of moisture absorption and desorption rates in PV modules. In Chapter 5 diagnostics for field testing are introduced. These include the identification of field degradation mechanisms in a set of CdTe thin-film modules, an analytical method for data filtering and thermal modeling of building-integrated PV (BIPV) facades to predict thermal stress. Chapter 6 presents conclusions on the entire thesis.

2. Photovoltaic cells and modules

2.1. Operating principles and performance

The active material in most solar cells consists of semiconducting layers which absorb sunlight. The absorbed energy is converted to electric current by separating released electrons from holes at a pn-junction between n- and p-type semiconducting materials. The n- and p-doping properties can be intrinsic (which is the case in thin-film solar cells), or they can be achieved with extrinsic doping by incorporating specific dopant atoms into the base semiconductor. The pn-junction is created when n- and p-type materials are joined together, as free electrons from the n-side move across the junction to fill the available holes on the p-side. This gradually creates an electric field since the charge difference between atom nuclei is exposed after electrons have moved across. The region where the electric field acts is called the space-charge region (or depletion region).

Sunlight photons excite electrons from the valence band to the conduction band on both sides of the junction, and charge carriers from each side are driven across the junction unless they have enough time to recombine. A key determinant of solar cell efficiency is therefore the recombination rate of charge carriers. Recombination can occur radiatively, through intermediate energy states in the bandgap or through Auger recombination between the energy bands [8]. In thin-film solar cells recombination through energy states in the bandgap is normally the performance-limiting mechanism since the density of such states is high.

To extract power from a solar cell, a voltage has to be applied across its poles. The relation between current I and voltage V in an illuminated solar cell is its key performance characteristic. The IV-curve corresponds to a diode curve offset along the current axis by the light-generated current. The IV-curve for a very good solar cell is shown in Figure 2.1. The cell should preferably operate close to the point where its power is maximized, indicated in the figure. This point is defined by the maximum power point voltage V_{MPP} and the maximum power point current I_{MPP}. Also indicated in the figure are the short-circuit current I_{SC} and the open-circuit voltage V_{OC}. These four parameters, together with the fill factor (FF) defined in Figure 2.1, are the basic performance parameters of solar cells and modules. In general, I_{SC} depends linearly on the irradiance G with a sensitive spectral dependence, while V_{OC} is usually proportional to the logarithm of G and not very sensitive to the spectrum.

The efficiency η of a PV device can be written as

$$\eta = \frac{P_{MPP}}{G \cdot A} = \frac{FF \cdot V_{OC} \cdot I_{SC}}{G \cdot A}, \tag{2.1}$$

where P_{MPP} is the maximum power and A is the device area. Cell degradation manifests itself as a decrease in efficiency. More detailed information on the degradation mechanism is obtained if it can be correlated with changes in one of the parameters I_{SC}, V_{OC} or FF. Common degradation mechanisms which reduce I_{SC} include increased resistive losses, while V_{OC} is reduced if shunt currents bypass the pn-junction. Shunts

can be produced by impurities and interfaces in the cell. Both resistive and shunting loss mechanisms usually also influence FF adversely. In basic IV-curve analysis these losses are represented as two resistance quantities, series resistance R_S and shunt resistance R_{SH}.

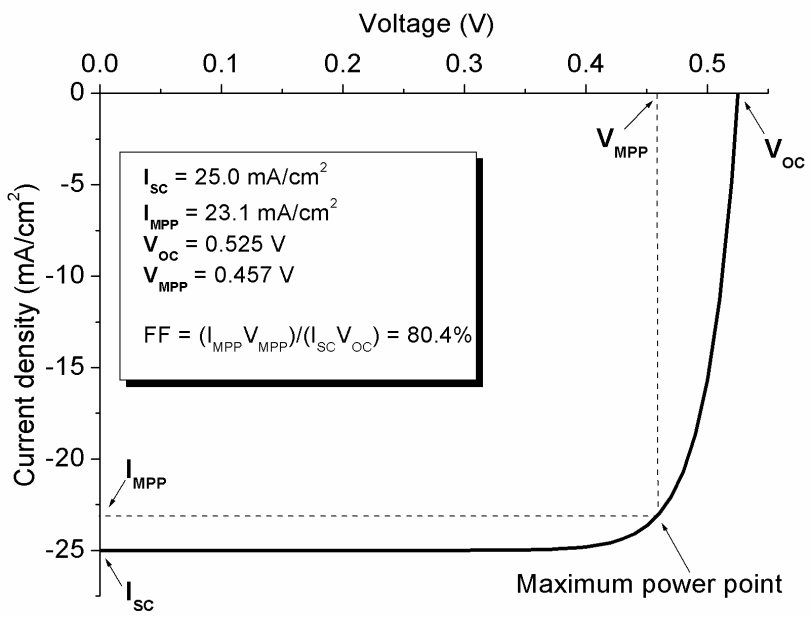

Figure 2.1: The IV-curve of a solar cell with characteristic parameters indicated.

In an ideal cell there are no resistive losses and no leakage currents past the junction. In this case $R_S = 0$ and $R_{SH} \rightarrow \infty$. The effect of resistance changes on the ideal solar cell IV-curve is illustrated schematically in Figure 2.2. The magnitude of the changes will depend on the characteristics of the cell in question and the severity of the degradation. It is seen that changes in both R_S and R_{SH} reduce the fill factor of the cell as the IV-curve flattens.

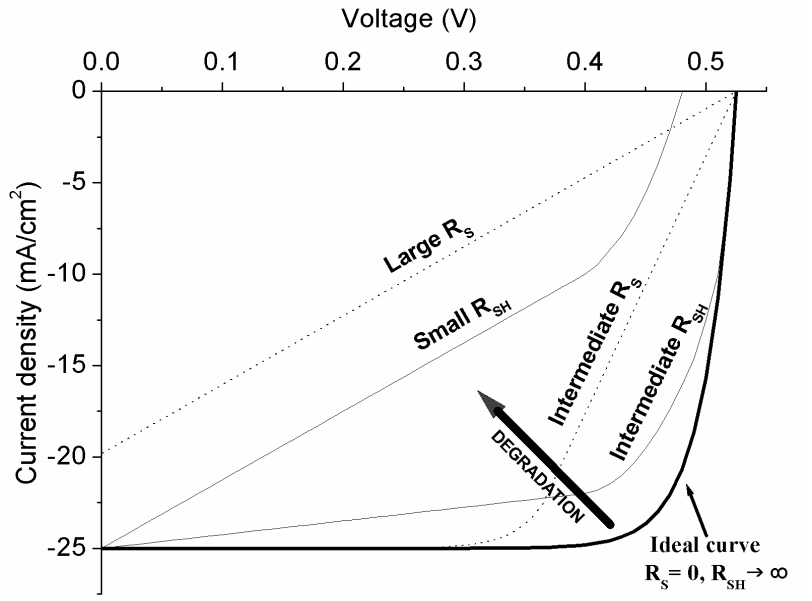

Figure 2.2: The effect of series and shunt resistance on the ideal IV-curve.

The upper efficiency limit of an ideal single-junction solar cell can be deduced theoretically as a function of the semiconductor bandgap. The bandgap is the most important efficiency-restricting factor, because incident sunlight is not monochromatic. Photon energy is therefore lost in a solar cell through the following loss mechanisms:

1. Photons with energy less than E_g do not generate any charge carriers in the cell.
2. The excess energy of photons with energy larger than E_g is lost, since the carriers immediately thermalize to the bottom of the conduction band.

Additional loss factors which cannot be avoided are [9]:

3. At nonzero temperature a solar cell emits thermal radiation to the environment. This limits the open-circuit voltage to a value smaller than the bandgap voltage E_g/q, where q is the elementary charge.
4. Nonzero current always reduces cell voltage, so V_{MPP} has to be less than V_{OC}.

The theoretical maximum efficiency for a single-junction solar cell with an ideal bandgap close to 1.5 eV illuminated by the AM1 solar spectrum is limited by the above mentioned factors to just over 30% [9]. Additional loss factors such as reflection of light at the top surface, recombination losses at interfaces, imperfect absorption of photons within the semiconducting material and incomplete collection of carriers released far from the junction all contribute to lower the achieved efficiencies further.

At the time of writing, cell efficiency records for the most common solar cell types stand at 24.7% for crystalline silicon (c-Si) and 20.3% for multicrystalline silicon (mc-Si). Thin-film solar cell records are 18.4% for $Cu(In,Ga)Se_2$ (CIGS), 16.5% for CdTe and 12.1% for (triple-junction) amorphous silicon (a-Si) [10]. All of these records have been achieved with laboratory-scale cells with areas of 1–4 cm^2. When individual cells are connected together to produce a module, the module efficiency will inevitably be lower than cell efficiency. This is caused by the 50–150 cm^2 cell size required for module use, by the additional resistance in the cell interconnections and by the mismatch between the characteristics of individual cells. Module efficiency records are currently 22.7% for c-Si, 15.3% for mc-Si, 13.4% for CIGS, 10.7% for CdTe and 10.4% for (triple-junction) a-Si [10]. The areas of the record modules ranged from 780 cm^2 (c-Si) to 4900 cm^2 (CdTe).

2.2. Thin-film photovoltaics

The focus of this thesis is on the development of methods for stability studies on thin-film photovoltaics. The primary driving force behind the development of thin-film solar cells has been the conviction that they can produce significantly cheaper PV electricity than the c-Si and mc-Si technologies which dominate the market today. Expectations of low costs are justified especially by the difference in production methods, as thin-film module manufacturing can be automated to a fast pace production sequence more easily than c-Si or mc-Si manufacturing. It has been estimated that thin-film PV production becomes cheaper than c-Si/mc-Si production when the total module power produced in the PV factory exceeds 20 MW/year [11], but at the time of writing thin-film PV factories are still clearly below this limit.

The primary component in thin-film solar cells is the absorber layer, which is a few μm thick. Adjacent to the absorber a second, thinner layer of semiconducting material is deposited to create the pn-junction. This layer is referred to as the window layer since it normally has a wide bandgap which allows nearly all energetic photons to pass through it. The front contact of a thin-film solar cell has to be transparent (usually a transparent conducting oxide, TCO) while the back contact can be metallic. Figure 2.3 shows schematically the stack of deposited layers on the substrate for the standard configuration of the three thin-film technologies. It can be noted that the CdTe cell presented in Figure 2.3 is in a superstrate configuration where light passes through the substrate before it enters the cell. CIGS and a-Si are in the opposite, substrate configuration. The former configuration requires a transparent substrate, whereas the encapsulation polymer has to be transparent in the latter configuration. Cells can be made in opposite configuration to the ones shown in Figure 2.3, but in the case of CdTe and CIGS this gives cells with clearly lower efficiency.

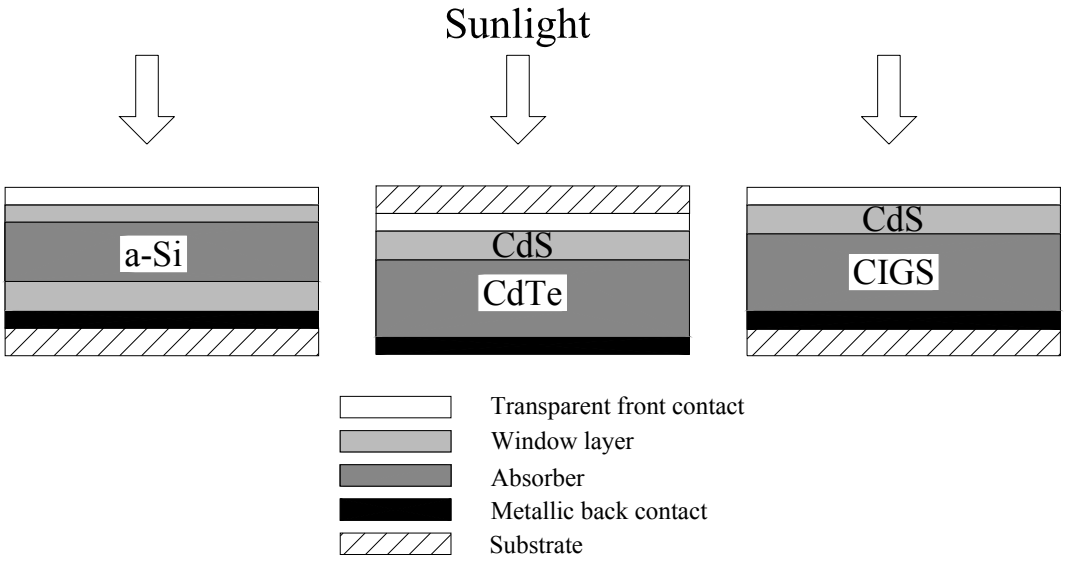

Figure 2.3: Cell structures for a-Si, CdTe and CIGS thin-film solar cells. CdTe cells are made in the superstrate configuration while a-Si and CIGS are in substrate configuration. Layer thicknesses are not to scale.

The window layer is normally n-type CdS in CdTe and CIGS cells, where the absorbers are p-type metal-semiconductor compounds. Amorphous silicon cells are made in a p-i-n structure where the a-Si material is surrounded by a p-type layer on one side and an n-type layer on the other side. Both of these layers are usually amorphous silicon compounds with suitable doping elements included, such as carbon. a-Si cells can also conveniently be manufactured as tandem cells, where different layers absorb separate parts of the solar spectrum. A number of alternative transparent and metallic contacts are possible for each thin-film cell type [12].

Degradation can occur in any of the cell layers. The polycrystalline or amorphous absorber and window materials have a high density of crystal defects. New defects can be created by stress factors. Energy states in the middle of the bandgap can have particularly significant impacts on cell performance. The understanding of defects, grain boundaries and their sensitivity to stress factors is crucial in the development of stable,

high-efficiency thin-film solar cells. In the contact layers, resistance loss is the foremost degradation concern. The interfaces between different layers in the cell are also highly important from a stability perspective. The window/absorber, absorber/back contact, window/front contact, back contact/substrate interfaces can all be vulnerable to degradation. Degradation mechanisms are discussed in detail in Chapter 3.

2.3. From cells to modules

Before a module is deployed outdoors the cells also have to be protected with a suitable encapsulation. Before that, cells need to be connected in series to make a module with enough voltage to do useful work. The structures shown in Figure 2.3 represent single cells, which usually have an open-circuit voltage between 0.5 and 1 volts depending on the bandgaps of their materials. These encapsulation and series connection phases have important implications for module stability.

Protecting the active parts of the module from the environment is a highly important part of module manufacturing. This is normally performed with an elastomeric polymer encapsulant (usually ethylene-vinyl-acetate, EVA) in a vacuum lamination process. The encapsulant acts as an adhesive between the front and back sheets and protects the cells. Figure 2.4 illustrates the encapsulation of a thin-film PV module and that of c-Si / mc-Si modules. In thin-film modules the active materials are deposited on the back or front sheet and the encapsulant polymer is laminated between the two sheets. In silicon modules, cells are laminated between two separate encapsulant layers.

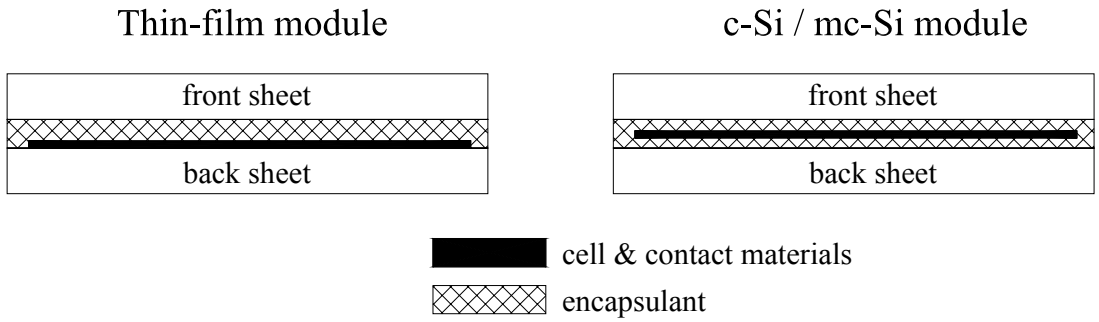

Figure 2.4: Comparison between the encapsulation structure of thin-film PV modules and of crystalline silicon modules.

From a stability perspective, the primary task of the encapsulant is to stop water, air and impurities from corroding the cells. The difference between thin-film and silicon module encapsulation illustrated in Figure 2.4 may be important in this respect, because water diffusion at the interface between encapsulant and glass may be quicker than in the bulk of the encapsulant [13]. The adhesion of the polymer to the substrate and the active materials is a factor of great importance for stability in both module types. The role of encapsulation in module stability is discussed in more detail in Chapter 3. The moisture sensor developed in this thesis for water diffusion measurements in encapsulated structures is presented in Chapter 4.

Connecting multiple cells together to form a module produces devices with high currents and voltages, but it also introduces new functional parts which are often sensitive to external stress factors. Thin-film modules are prepared by separating deposited films into single cells during the manufacturing process. This requires a scribing phase after each deposition step. The basic sequence is illustrated in Figure 2.5 for the case of a CIGS module with four cells, with different layers colored according to the convention chosen in Figure 2.3. The sequence proceeds as follows:

1. The back contact molybdenum is first deposited over the entire substrate. Electrically separated areas, usually approximately 10 mm wide, are defined by laser scribing at the positions indicated with arrows.
2. The CIGS and CdS materials are deposited over the entire substrate, covering the previous scribe lines. New scribe lines are made through these layers down to the molybdenum layer.
3. The transparent front contact is deposited across the module area and scribe lines are drawn down to the molybdenum at the locations indicated by arrows. This completes the module with four separate cells.

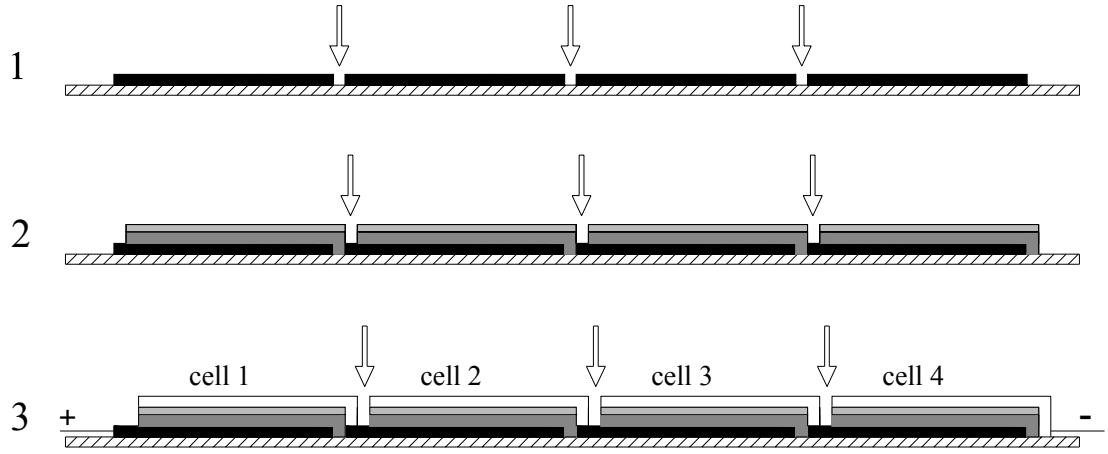

Figure 2.5: Illustration of alternating deposition and scribing to create a CIGS module with 4 cells connected in series. Arrows indicate the scribe lines drawn after the deposition step. Layers are coloured as in Figure 2.3.

In practice, the scribe lines of one interconnect cannot be drawn precisely adjacent to each other as in Figure 2.5. They are usually spaced about 0.5 mm apart. From a stability perspective, it is important that the resistance at the front/back contact interface does not increase and that the CIGS layer keeps the back contacts of adjacent cells electrically isolated from each other. It has also been suggested that preferential penetration paths for moisture may develop along the length of the scribe lines if the adhesion of the encapsulation polymer to the interconnect is imperfect [13]. This makes corrosion resistance at the interconnects an especially important issue.

3. Stability of thin-film PV modules

Photovoltaic modules can be used nearly everywhere across the globe. Environmental factors such as rain, snow, dirt and UV-light, and other factors such as high voltages between modules and their frames can potentially influence their operation. The peak temperature of PV modules can be as high as 70°C. On sunny days the difference between daily maximum and minimum module temperatures is at least 30°C in most locations and as much as 60°C in extreme conditions. During continuous operation for up to 20–30 years, these factors place a significant stress on all parts of the PV module. Stability improvements require detailed understanding of the relation between external stress factors and module degradation.

Several aspects of thin-film PV modules can be studied from a stability perspective. Most attention is usually given to the study of single unencapsulated cells. Cell studies can be undertaken early on in the development of new technologies when a lot of experimentation is done with different cell structures. At this stage stability during thermal stress and under UV-light are the most important issues, since failure to meet those criteria would immediately rule out the cell in question from outdoor use. The thin-film cells being developed today meet these requirements, but many of them are sensitive to moisture. Studies in humid conditions are therefore a very important part of cell development.

When the step from cell studies to module testing is taken, the module integration issues presented in section 2.3 bring additional stability challenges. The interconnect regions between individual cells are important functional parts of the module and corrosion or impurities can create shunts between adjacent cells or increase the resistance between them. The importance of interconnect degradation mechanisms can be evaluated in the laboratory. Humidity testing and thermal cycling are among the most important tests. The encapsulation of the module directly determines the amount of exposure to moisture and impurities. Polymers can undergo changes both due to thermal stress and UV-light. These changes may affect the rate at which moisture and impurities penetrate the module. The relation between stress and degradation is therefore a combination of the encapsulation quality and the sensitivity of the active materials.

Finally, field testing is the final step in evaluating module stability. Modules deployed in field tests have normally passed several stages of accelerated aging in the laboratory. The primary objective in field testing is to discover which degradation mechanisms limit module performance in real operating conditions. Feedback from field testing can then be used both to improve stability and to fine-tune the accelerated aging tests needed to study the dominant field degradation mechanisms. Based on this knowledge, the goal should ultimately be to predict the field lifetime of a module from the results of the accelerated aging test.

This chapter begins with a brief description of commonly used accelerated aging tests for thin-film photovoltaic modules and continues with a review of stability questions for thin-film CdTe, CIGS and a-Si cells and modules. Degradation mechanisms which have been identified in earlier work are presented. The relation of accelerated aging results to outdoor degradation is also discussed. Mechanical stability issues such as glass breakage or warping are not included in this review.

3.1. Accelerated stability testing

Accelerated aging tests are conducted in the laboratory where experiments can be performed in a controlled and repeatable way. Degradation mechanisms can be studied by applying stress factors to the cells/modules separately or simultaneously. Standardized PV module qualification tests which specify procedures and passing criteria have been developed in order to ensure that the modules on the market meet customer requirements for stability and lifetime [14–16]. The benefit of having standardized tests is that module designs can be tested easily and a basic lifetime estimate can be made upon successful completion of the test. A possible disadvantage is that stability goals are sometimes set only with the aim of passing standardized tests. The relevance of the tests for real outdoor stability is then taken for granted. The standards mentioned above are primarily based on experience gained from c-Si and mc-Si module testing. Their suitability for thin-film module qualification can be questioned [17]. However, the existing standards still give a general idea of the required stress magnitude in accelerated aging tests. The tests which are relevant for this thesis are presented below.

High temperature tests are not included in standardized test procedures, but are often used in cell development. They are usually conducted at temperatures between 80°C–120°C in a dry atmosphere. It is often of interest to repeat the test at several temperatures. High temperature testing is sometimes combined with light soaking. In addition to testing light stability, light soaking can be used to test the influence of voltage bias on the module.

Temperature cycling is conducted between –40°C and +85°C in the IEC thin-film module qualification standard, with 50 or 200 cycles and a 4 hour cycling period. It is complemented by a humidity freeze test where modules are kept at 85°C and 85% relative humidity (RH) for 20 hours, followed by –40°C for 1 hour. This humidity freeze cycle is repeated 10 times in the IEC test sequence [15].

High temperature and humidity are combined in the damp heat test, conducted at 85°C and 85% RH. In the IEC thin-film test standard, the duration of the test is 1000h [15]. The test is primarily conducted on encapsulated modules, but unencapsulated cells are also often tested in these conditions to study moisture-induced degradation mechanisms in more detail. Comparisons between results from high temperature tests, damp heat tests without encapsulation and damp hest tests with encapsulation are often a useful way to distinguish between different degradation mechanisms.

The influence of high voltages on module stability can be studied on its own or in combination with high temperatures. Voltages as high as 500 V are needed to replicate the highest possible voltages between a module and its metallic frame in a system of several series-connected modules. Voltage testing is not included in standardized tests.

High temperature testing can be conducted in ovens, whereas the combination of temperature and humidity requires a climate chamber. In the work conducted in this thesis, Arctest ARC-150 and ARC-400 climate chambers were used in the tests where temperature and humidity had to be controlled.

3.2. Overview of thin-film PV degradation mechanisms

In Table 3.1 a compilation of thin-film PV module degradation mechanisms is presented (adapted from [7]). The stress factors which can cause the degradation are also indicated.

Table 3.1: Thin-film PV degradation mechanisms and the stress factors which can cause them; high temperature, temperature cycles, UV-light, moisture, high voltages and the presence of impurities.

Cell-level	High T	T cycl.	UV	H_2O	High V	Impur
C1. Transport of species and creation of defects - Increase in R_S / Decrease in R_{SH} / Weaker electric field	•		•	•	•	•
C2. Formation of blocking back contact (CdTe) - Roll-over in IV-curve / Increase in R_S	•			•		
C3. Corrosion in contact layers - Increase in R_S	•			•		•
Module-level	High T	T cycl.	UV	H_2O	High V	Impur
M1. Corrosion and electromigration at interconnects - Increase in R_S	•			•	•	•
M2. Shunting between contacts in interconnect region - Decrease in R_{SH}	•			•		•
M3. De-adhesion of front and back contact from substrate - Increase in R_S	•	•		•	•	•
M4. Water diffusion through encapsulant	•			•		
M5. Delamination of encapsulant	•	•	•	•		•
M6. Photothermal degradation in encapsulant polymer - Loss of transparency	•		•			

The importance of temperature and humidity stress is evident in Table 3.1; all degradation mechanisms can be expected to occur faster at higher temperatures and the presence of water can damage the cell or module in many different ways. Thermal cycling can cause encapsulant delamination or damage the interconnects. It is important to note that some degradation mechanisms can be self-reinforcing: water penetration may cause encapsulant delamination, which makes it even easier for additional water to penetrate the module at the glass/encapsulant interface.

Cell stability can be considered technology-specific since there are significant differences between CdTe, CIGS and a-Si cells. There are also differences within each technology, since changing contact materials or layer thicknesses in thin-film cells can influence stability markedly. This is the case especially for CdTe and CIGS cells where the search for a final 'best' cell design is to some degree still in progress. At the module-level the encapsulation issues are in general the same for all thin-film

technologies, except that encapsulant transparency is not needed in CdTe superstrate devices. Interconnect stability, on the other hand, is to some degree technology-specific because the contact materials are different.

For the purposes of this thesis, mechanisms C1–C3 and M1–M4 are relevant. Mechanisms M5 and M6 depend on the physical and chemical properties of the encapsulation polymer. They are beyond the scope of this thesis and are dealt with only in conjunction with other degradation mechanisms below. In the following review of the present status of thin-film PV degradation research, studies on mechanisms C1 and C2 in Table 3.1 are presented on a technology-specific basis. The other degradation mechanisms have not been studied to the same degree for all technologies, so all of the available studies are included under the same heading.

3.2.1 Transport of species and creation of defects (C1)

An ideal solar cell would retain its internal structure throughout its lifetime. However, high temperatures and electric fields produce atom and ion transport in all solar cells, and new lattice defects are continuously introduced. The tendency for diffusion and electromigration is determined by the mobility of the atomic species in the solar cell (lattice atoms, contact materials, dopants and impurities) and by the electrical environment surrounding them. Defects may also be created if impurity atoms enter the solar cell from the outside, a mechanism which depends on the protective properties of the encapsulant. The literature on these stability aspects is reviewed below for each thin-film solar cell technology.

CdTe

Polycrystalline p-type CdTe has an ideal bandgap for photovoltaic energy conversion, but it also has a property which has led to problems in stability. Its work function is approximately 5.7 eV [18], which makes it impossible to contact it ohmically with a metal. This back contact problem is dealt with in more detail when degradation mechanism C2 is discussed, but the solutions have a significant impact on mechanism C1 as well. The contacting problem can be adequately solved by using copper to dope the CdTe surface prior to contacting. With Cu and graphite the back contact becomes as good as ohmic when a Cu_2Te layer is created at the back contact interface [18]. However, copper is a very mobile atomic species. In CdTe cells it can readily diffuse especially along grain boundaries and act as a recombination center close to the pn-junction. Copper escape may also make the back contact non-ohmic again. If copper begins to populate the CdS layer, it can increase the photoconductivity when present in small amounts, but eventually it will decrease the donor concentration and lead to increased recombination [18].

The effect of voltage (cell voltage or external voltage) can be significant in promoting CdTe cell degradation because the electric field will contribute to driving copper ions towards the front contact at forward bias [19, 20]. This may partly explain the severity of degradation which has been observed in previous studies in open-circuit / forward bias compared to degradation under different bias [21–23]. To some extent, the presence of chlorine in the CdTe/CdS cell after $CdCl_2$ treatment has been thought to cause similar degradation as Cu [18]. However, in more recent work the role of Cu and chlorine

diffusion in the initial stages of cell degradation has been considered small in comparison to oxidation processes [24]. The interdiffusion of the CdTe and CdS films is another degradation mechanism which has been mentioned as a possible cause for performance decrease under high-temperature stress [18, 24].

Copper-free back contact solutions for CdTe cells have also been developed [25]. Recent studies indicate that diffusion and migration of dopants and impurities can cause stability problems in such cells also. In [26], two kinds of cells with Sb_2Te_3/Mo back contacts were tested in high-temperature (100^{o}C, 1 sun illumination) conditions. Cells with glass/ITO/SnO_2 front contacts improved their performance during the test, whereas cells with Cd_2SnO_4/In_2O_3 front contacts degraded markedly. The degradation in the latter was attributed to the diffusion of dopant atoms away from the pn-junction, which weakened the electric field. These results indicate that the front contacts of CdTe cells may also affect stability in surprising ways.

An entirely different aging mechanism is presented in [27]. A metastable shunt at the edge of the CdTe cell was found to be induced by voltage, humidity and temperature. This may have significant implications for module design since scribe lines create numerous locations for this degradation mechanism to develop.

CIGS

Based on the detrimental effect of copper on the stability of CdTe cells, a sceptical attitude toward the stability of Cu(In,Ga)Se_2 solar cells may initially seem justified. However, it has been thoroughly argued that copper atoms do not pose stability problems for CIGS cells because CIGS material has a flexible structure which makes it very tolerant to chemical changes in its environment [28–31].

Two properties of CIGS material are particularly important for its chemical stability. Deviations from the basic Cu(In,Ga)Se_2 stoichiometry can be fairly large in the absorber material, which creates an abundance of intrinsic defects such as interstitials, vacancies and substitutional atoms in the CIGS lattice. However, most of the energy levels associated with these intrinsic defects are shallow defects close to the conduction or valence bands, or are situated outside of the bandgap [30]. This gives the CIGS material a flexible nature without limiting performance. The second beneficial property is that the chemical potential of Cu^+-ions confines them to the CIGS absorber where they do not degrade the electrical properties of the material, but instead act as defect passivators [30]. An elegant example of this mechanism in action is the neutralization of ionized defects caused by radiation. Copper interstitials and vacancies act quickly to restore electrical equilibrium in the material [28].

Testing of unencapsulated CIGS cells in damp heat conditions has indicated that humidity degrades cell performance under prolonged exposure. Degradation manifests itself both in V_{OC} and FF loss. The degradation process appears to be a complex one and several different changes have been observed in the cells. Fill factor degradation results in part from a decrease in the conductivity of the transparent ZnO front contact, which also increases the barrier electrons must cross when moving from the CIGS layer to the CdS layer. Increased concentration of deep acceptor states in the CIGS absorber probably plays a role in both V_{OC} and FF degradation [32].

In other studies, donor-type defects have been found more important in explaining both of these losses [33]. A key question is the identification of the defects, which would clarify which components in the CIGS lattice interact with H_2O or OH-groups. This issue has not been settled yet and the answer may indeed be cell-specific. In the case of $Cu(In,Ga)(S,Se)_2$ cells, V_{OC} and FF degradation can occur due to sulfate formation at interfaces [34–36], but this is probably not a relevant degradation mechanism in $Cu(In,Ga)Se_2$ cells. Other studies on damp-heat tested CIGS cells have dealt with the influence of Ga-content on cell stability [37], and optical microscopy of the surfaces of stressed cells has been performed [38].

a-Si

The performance of amorphous silicon cells and modules degrades when they are exposed to sunlight. The performance stabilizes at a level which is approximately 70–80% of the initial value. Since the degradation occurs within a few weeks or months of outdoor use, this stabilized performance can be regarded as the true operational performance. The degradation mechanism responsible for performance loss is called the Staebler-Wronski effect. After degradation, cell performance can be restored by annealing at high temperatures. Cycles of degradation and improvement have been observed in field operation. Annealing can also be used in the manufacturing process to improve module quality. The physical explanation for the degradation is thought to be the increase of metastable 'dangling bond' defects. These are atomic bonds of silicon atoms which are not attached to neighbouring atoms due to the lack of lattice structure. Such irregularities create an abundance of recombination centers within the bandgap. The stabilization of performance can be explained as a balancing of defect creation and annealing.

Theoretical explanations for the Staebler-Wronski effect have been presented [39], but a complete consensus on the degradation mechanism is still missing [40]. While no method for eliminating the Staebler-Wronski effect has been found yet, there are several ways of reducing the magnitude of degradation. These include the use of buffer layers [41], optimization of film growth conditions from a stability perspective and the use of textured substrates and reflectors which allows a thinner film with less recombination loss [40]. In addition to the Staebler-Wronski effect, the possibility of performance degradation in a-Si cells due to Al diffusion from the back contact and texturing layers has been investigated [42,43].

3.2.2 Back-contact blocking in CdTe (C2)

The characteristics of metal/semiconductor interfaces depend on the work functions of both materials. When the contact is created, the Fermi levels are equalized and the energy bands bend (downward, in the case of a p-type semiconductor) at the interface to accommodate the alignment of vacuum energy levels. If the work function of the semiconductor is greater than that of the metal, this band bending creates a barrier for charge transport at the interface. This is the case for CdTe because no metal with a work function larger than 5.7 eV is known today. Solutions to this problem have been sought by creating a strongly p-doped layer at the CdTe surface before contacting. When it is successfully carried out, this procedure reduces the barrier height to allow significant tunnelling of charge carriers through it. Doping has been carried out successfully with

doped graphite paste, forming interlayers such as Cu_2Te and $Hg_{1-x}Cd_xTe$ at the back contact interface and making the contact quasi-ohmic [18].

Implications of the introduction of metallic species on cell stability were discussed in section 3.2.1., but the quasi-ohmic contact can also degrade cell performance markedly if oxidation occurs at the contact interface. A theoretical model for CdTe cell degradation due to oxidation at the back contact has been proposed by Singh et al. [44]. They modeled the oxidized contact as a metal-insulator-semiconductor system. In cells with Cu-based back contacts, the contact can become severely blocking as Cu moves into the cell and the doping at the back junction is reduced, as shown in high-temperature tests [20]. In other work, cell degradation in hot and dry conditions has been attributed primarily to the formation of an insulating $CdTeO_3$ layer at the interface due to oxygen migration through the back contact metal [19]. The penetration of water into the cell is known to hasten the formation of the blocking back contact significantly.

More recent work on back contacts with Sb or Sb_2Te_3 buffer layers has yielded good stability even in humid conditions [45], although the work presented in this thesis shows that such modules may suffer from other degradation mechanisms in the field (Chapter 5). A comparison of efficiency and cell stability between some Sb-based and Cu-based back contacts has been presented [46]. In addition, it has been suggested that rollover in the IV-curve may also depend on the transparent front contact [25]. It is also of interest to note that rollover has been observed in $CuInSe_2$ cells [47] where it contributes to decreasing cell performance in accelerated aging tests. Results show that this mechanism is not related to the Mo back contact [48], but probably to changes at the $CuInSe_2$/CdS interface. However, the details of this degradation mechanism are unknown to date.

3.2.3 Contact and interconnect degradation, leakage currents (C3, M1–M3)

In addition to degradation within the active cell material, there are a number of module degradation mechanisms which can limit performance. Some of the most important ones are corrosion and electromigration in the contact layers and at the interconnects. Contact degradation mainly increases series resistance, while interconnect degradation may affect both series and shunt resistance adversely. Corrosive degradation can be electrochemical, where a voltage between an anode and a cathode (e.g. cell/contact materials and a metallic module frame) leads to leakage current and chemical changes in the cell/contact material. Other corrosion mechanisms include galvanic corrosion between two dissimilar materials (at the back/front contact interconnect interface, for example) and oxidative corrosion due to water penetration.

An electrochemical corrosion mechanism which has recently been identified is the delamination of transparent SnO_2 contacts from soda-lime glass substrates. This mechanism is caused by an electric field between module and frame, which drives sodium ions from the glass to the interface between SnO_2 and glass. If water then penetrates the module, the bonding at the interface may become weaker and delamination of the SnO_2 contact may occur [49]. The presence of water vapour also decreases the resistance for leakage current, which further accelerates the degradation. It has been observed that the degradation occurs only when the TCO is biased negatively

with respect to the metallic frame and that modules without frames do not show this degradation mechanism [50]. Approaches toward solving these problems focus on using different glass substrates or different TCO front contacts, such as ZnO which appears to be more durable in this respect [49].

The above work builds on the electrochemical testing of thin-film modules performed at the Jet Propulsion Laboratories (JPL), which included lifetime predictions based on measurement of transferred charge between module and frame, and studies of the effect of the encapsulant on electrochemical degradation [51–53]. In addition, the influence of temperature and humidity on leakage current was investigated [54]. In the JPL studies, galvanic corrosion in a-Si modules was also a research topic, with a focus on the TCO/back contact (in this case SnO_2/Ag) interconnect and the interface between aluminium metallization and glass. The results from the former samples showed no galvanic corrosion, while observed corrosion in the latter samples did not yield a significant increase in resistivity. CdTe and CIGS modules have different interfaces and would require separate studies. Galvanic corrosion has not been identified as a problem in thin-film modules to date.

In the case of oxidative corrosion due to water exposure, increased resistance in the contact layers is a commonly observed effect in damp heat testing [32], but problems can often be amended by changing layer thicknesses [55]. The corrosion resistance of the interconnects, where current is transported along very thin regions, may be more difficult to manage. This topic was explored for CIGS modules in a study where the shunt and series resistances of unprotected cells, with and without interconnects, were monitored during damp heat testing. It was found that the increase of series resistance at the ZnO/Mo interface linking the back contact of one cell to the front contact of another is a viable explanation for the difference between module degradation and cell degradation [56]. A more detailed analysis of CIGS contact and interconnect loss mechanisms and suggestions for module optimization for long-term stability were given by the same authors in a later publication [57]. In a more recent study it was observed that a significant increase in ZnO sheet resistance during damp heat testing occurs in $CuInS_2$ modules, but not in $Cu(In,Ga)Se_2$ modules. The effect of interconnect design on the moisture sensitivity of the ZnO/Mo interface was investigated in the same paper [58].

The final degradation mechanism to be dealt with here is electromigration, caused by high current densities when momentum transfer activates the diffusion of contacting materials. Again, it is not likely to be a problem in contact areas surrounding the cell, but sufficiently high current densities can occur at the interconnects if they are too narrow. Electromigration has been studied at JPL [59, 60]. In the tested samples, exposure to current densities as high as $3 \cdot 10^4$ A/cm^2 at 82^{o}C for 2000h did not produce degradation effects with significance for 30 years of outdoor operation. It seems plausible that thin-film PV module interconnects can be designed to keep current densities below the experimental threshold for electromigration [60].

3.2.4 Water penetration and module encapsulation (M4)

As shown in Table 3.1 and in the presentation of degradation mechanisms given above, water penetration into a thin-film module can be a driving force for many mechanisms. In addition to being a corrosive impurity, water can increase leakage current by reducing the charge transfer resistance between the active components of a module and the module frame. It may also reduce adhesion between the encapsulant and the substrate, which facilitates further water penetration. In a JPL study on water penetration mechanisms, it was suggested that thin-film PV modules are more vulnerable to water penetration than c-Si or mc-Si modules because the thin-film active material is located at the encapsulant/substrate interface, whereas c-Si and mc-Si are surrounded by the encapsulant on all sides [13]. In addition, the scribe lines which separate cells from each other in a thin-film module may provide pathways for humidity.

In an extensive study of thin-film PV lifetime testing, the damp heat test was found to be the most stringent accelerated test for a-Si, CdTe and CIGS modules. Significant moisture ingress was observed at the module edges, in some cases with clear evidence of corrosion both in the visible contacts and at the interconnect lines. In a-Si modules FF degradation was the foremost degradation symptom, suggesting an increase in series resistance during the test. CdTe and CIGS modules showed degradation in all performance parameters, indicating a more complex pattern of degradation [17]. As presented in sections 3.2.1 and 3.2.2, humidity can affect the performance of CdTe and CIGS modules in multiple ways. It can also be observed that results presented in Publication III of this thesis show that some CdTe modules, in this case with low efficiency, can withstand the damp heat test even when unencapsulated. This is an example of how the stability of thin-film modules can be highly dependent on the details of cell structure and design.

A key goal in thin-film PV protection is finding an encapsulation solution which gives as little water exposure as possible combined with good adhesional stability at the interfaces. These issues are discussed in [7] and recent material testing at the National Renewable Energy Laboratory (NREL) is presented in [61, 62]. Another important issue is encapsulant stability, since polymers are susceptible to chemical changes when exposed to high temperatures and UV-light. A number of studies have been conducted on the stability of ethylene vinyl acetate, the most widely used PV encapsulant today [63–66].

Photovoltaic encapsulation research is a broad field which includes the study of elastomeric polymer encapsulants, polymeric front- and backsheet materials, edge sealants and barrier coatings. It is likely that the glass/cell/EVA/glass module configuration will eventually be replaced in thin-film PV modules, possibly through the use of flexible front- and backsheets, new encapsulant polymers or multilayer encapsulation solutions with specifically engineered barrier films. For the purposes of this thesis, the central issue is that polymeric encapsulants are likely to remain a vital part of PV encapsulation for the foreseeable future and that the diffusion of water through the encapsulant is the catalyst of a number of degradation mechanisms. The measurement and modeling of this diffusion process is an issue which has received little attention in PV research to date.

The basic water protection parameter of the encapsulant is its water vapor transmission rate (WVTR), which is measured from free-standing films. While the WVTR value gives an initial indication of the water-protection properties of a given encapsulation material, there is a strong need to measure and model water diffusion in actual PV module encapsulants to study questions such as i) the distinction between bulk diffusion and interfacial diffusion, ii) alternating water penetration and escape from the module in wet and dry conditions, iii) the amount of water needed for a given decrease in thin-film cell performance, iv) the influence of polymeric front- and backsheets or multi-layer encapsulants on the water exposure of the cell, and v) the relation between water penetration and encapsulant delamination. As a step in this direction, basic modeling of water penetration in different situations has recently been performed at NREL with the help of WVTR data [67], but the number of studies in this research area remains low.

3.3. Correlating accelerated aging tests with field tests

Most of the studies cited in section 3.2 were based on accelerated aging experiments conducted in laboratory conditions. As stated earlier, it is important to make sure that accelerated aging replicates only degradation mechanisms which occur in real operating conditions. Ideally, a test routine including multiple phases of field testing, laboratory testing and module improvement should be devised to achieve stable thin-film PV modules [6]. A lot of work has been performed in recent years to improve the understanding of thin-film PV field degradation mechanisms, but correlative studies between field and laboratory aging remain rare.

A significant number of studies have been published on long-term field testing of a-Si thin-film photovoltaic modules [68–70]. For CdTe and CIGS, the number of field studies is more limited [71, 72], but it can be expected to increase in the near future as the commercialization of these technologies proceeds. From the perspective of lifetime prediction, the utility of basic field measurements is limited unless some information on the degradation mechanisms responsible for performance changes in the module can also be gained. In some cases, such as the Staebler-Wronski effect in a-Si modules, field measurements can be interpreted as direct evidence of a particular mechanism at work, but this is usually not possible. For this reason, there is a need for specialized field testing designed to uncover specific degradation mechanisms and for sample analysis from degraded modules.

Leakage currents from both crystalline and amorphous silicon modules were studied in a three-year field test at NREL [73]. It was found that leakage current through the soda-lime substrate glass was the dominant mechanism in wet conditions, whereas conduction along the EVA/glass interface is an additional loss component in dry conditions. However, a direct correlation between performance loss and leakage current could not be established. In earlier work at NREL, a method for studying the shunt resistances of individual cells in complete, encapsulated modules was developed [74]. This was put to use in [75] on field-tested $CuInSe_2$ modules. In this study, the formation of hot spots in the cells was interpreted as a sign of localized junction failure, which caused the loss in module shunt resistance. In a follow-up study, the same authors studied samples from degraded modules with scanning electron microscopy and energy

dispersive X-ray spectrometry [76]. This is a rare example of microscopic studies on samples from field-aged thin-film PV modules, but it yielded little information of value and sample preparation methods were not described at all.

Studies on laboratory and field aging of CIGS modules with a new buffer layer material are reported in [77], but without emphasis on degradation mechanisms. Comparisons between the development of the Staebler-Wronski effect in a-Si modules tested in the field and in the laboratory have been reported in [78].

In a study conducted at the Florida Solar Energy Center on c-Si modules, samples were obtained by coring and EVA encapsulant adhesion and cell corrosion was studied. As will be discussed in Chapter 5, the question of obtaining undamaged samples from encapsulated thin-film modules is not trivial. The adhesional shear strength of EVA was found to be weakest at its interface with the c-Si cell. After 7 years of outdoor exposure, the shear strength was only 20% of the strength in unaged module samples [79]. Another aspect of EVA stability which has received attention is its discoloration due to oxidation, which degrades module performance since encapsulant transparency is compromised. This question has been studied in detail for both laboratory- and field-tested samples [80].

Regarding the question of moisture penetration and escape, two recent studies present visual evidence both for moisture penetration into PV modules during wet seasons and moisture escape during dry seasons [81, 82]. The encapsulant used in these modules is apparently not known to the authors. The need for understanding water penetration and escape mechanisms, discussed in section 3.2.4, is a critical issue for evaluating the lifetime of modules in the field. Once sufficient understanding of these mechanisms has been obtained, modeling of water penetration in the field can be carried out with methods developed for other applications [83].

A general issue related to field testing is that modules are seldom tested at multiple locations with different climates. There is always some uncertainty involved in extending results from one location to another, but they can be minimized with careful recording of relevant meteorological parameters at the test sites.

In conclusion, bridging the gap between accelerated aging tests and field tests will require a lot of work in the future. It is highly important that the laboratory results for module degradation mechanisms M1–M4 are compared with field test results from identical modules. Thin-film module stability is a complex combination of encapsulation, module design and a choice of materials. The long-term stability of full-size modules cannot be estimated or guaranteed based only on laboratory testing. In the case of cell degradation mechanisms such as C1 and C2, it is a primary objective to verify which mechanisms actually occur in real outdoor use. This is not always possible for each cell technology because accelerated stability studies are often conducted in an early stage of cell development to quickly test cell stability in the presence of the principal stress factors. Field test results are not available in such cases. This illustrates the importance of general testing standards specifically developed for thin-film cells and modules.

3.4. Diagnostics developed in this thesis

The work presented in this thesis bears directly on several of the key issues in stability improvement and lifetime prediction presented above. Understanding moisture penetration into encapsulated PV structures, identified as a key priority in section 3.2.4, requires measurement of water concentration inside encapsulated test structures. The sensor used in the measurement should be of micrometer thickness to ensure that the experimental situation corresponds to the actual situation of an encapsulated thin-film solar cell. For the same reason, measurement leads should be extremely thin so that no preferential moisture penetration occurs along them. A third requirement is that the sensor must withstand the lamination process and a fourth is that it must be able to detect very small quantities of water. This thesis describes the development and calibration of a moisture sensing element which meets all of these requirements and gives a signal when approximately 10 μg of water has entered it (Publication I). The moisture sensor element is applied to a study of water absorption and desorption rates in EVA-encapsulated structures at different temperatures (Publication II). This is an important issue to study if the water exposure of PV modules in the field is to be estimated.

The second part of the thesis focuses on methods for identifying degradation mechanisms in field-tested thin-film modules. This problem relates directly to the discussion in section 3.3. It is demonstrated that degradation mechanisms C1–C3 and M1–M2 can be studied by taking small-area samples from field-tested modules and characterizing them electrically. A degradation study is conducted on full-size CdTe modules (Publication III). The sampling of the thin-film module in a non-destructive way and the separation of interconnect and cell degradation mechanisms from each other are emphasized. In addition, the precision of field data analysis is improved with the development of a data filtering methodology, applied in this thesis to CIGS modules (Publication IV). The method enables a search for correlations between stress factors in the field and observed module degradation. Finally, a tool for predicting thermal stress in BIPV a-Si modules in different climates is presented (Publication V). As seen in Table 3.1, thermal stress is a key stability issue and predicting it is therefore a high priority in PV stability research.

In the following chapters, the key results of this thesis are presented in more detail with reference to the relevant publications included in the thesis.

4. Moisture measurement in PV module encapsulations

(Publications I, II)

Water penetration is a potential aging factor for PV modules in most climates. The challenge is to achieve sufficient protection at reasonable cost, usually with the added requirement of optical transparency on one side of the module. At the present stage of encapsulation development, elastomeric polymers laminated between front and back sheets are the standard method for protecting the active materials from the environment. Module structures illustrated in Figure 2.4, with glass/EVA/glass composition, are especially common among thin-film modules. In this sandwich, the behaviour of EVA determines the water protection properties since glass is impermeable to water.

Despite the widespread use of EVA and extensive knowledge of its material properties, very little is known about water diffusion processes in actual PV module structures. This is true for both outdoor use and accelerated aging tests. The primary reason for the lack of experimental data and consequent lack of theoretical understanding is that no suitable, non-invasive moisture sensors have been available for this application to date. In particular, the thinness of the polymer (usually 0.5 mm or less) and the need for very thin measurement leads combined with the high lamination temperature (over 150^{o}C for EVA) precludes the use of commercially available humidity sensors.

The moisture sensor developed in this work solves these problems by being integrated as a functional part on one of the glass surfaces. The sensor effectively mimics a thin-film solar cell in the sense that its active part is a film of micrometer thickness, deposited on a glass substrate and encapsulated. This makes it a particularly useful tool for studying moisture diffusion from a thin-film PV point of view, but several other applications are also possible.

4.1. Moisture sensor development and calibration

(Publication I)

The basic idea behind the moisture sensor developed in this work is to use nanoporous TiO_2 as the moisture-sensitive component and to measure the resistance of the TiO_2 film with an electrode structure patterned on conducting, indium-tin-oxide (ITO) coated glass. Due to its porosity, the TiO_2 film can absorb a lot of water relative to its volume. The ac-resistance of TiO_2 depends very strongly on the amount of water it contains. TiO_2 was chosen as the sensor material primarily based on reports of its successful use in atmospheric humidity measurements [84–86], while ITO-on-glass coatings were chosen due to their suitability for photolithographic patterning by etching in a HCl / HNO_3 solution. Direct measurement of EVA ac-resistance as an indicator of moisture content, a concept explored earlier [87], was also considered but the very high resistance of EVA made this approach impractical. Using TiO_2 had the additional benefit of separating the sensor from the encapsulant material under study, thus allowing the possibility of studying multiple encapsulation materials with the same sensor. EVA resistance is several orders of magnitude higher than the resistance measured from wet TiO_2 films, so the measurement of sensor resistance is not influenced by currents through the EVA material outside of the sensor. This is likely to

be true also in applications where other polymeric encapsulant materials are studied with this sensor.

4.1.1. Sensor preparation and measurement

Sensor preparation was performed as follows. A photoresist mask was created on the ITO glass surface with standard photolithographic methods and the glass was etched and cleaned to create a pattern of conducting ITO on the glass surface. Different electrode geometries with variations in dimensions were studied in the initial tests. A high priority was to make the electrode area as small as possible without losing measurement accuracy. The geometry chosen for the sensor is presented in Figure 4.1. The number of fork fingers has been reduced by half to maintain clarity. The width of the fingers and the distance between them was 150 μm, the minimum obtainable linewidth in the photolithographic process.

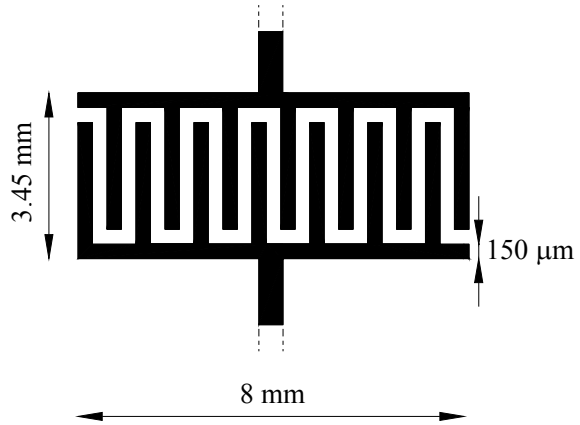

Figure 4.1: Geometry of the ITO-patterning for the sensor. The number of fingers has been reduced by half for clarity.

In Figure 4.1, the conductors leading away from the top and bottom indicate the ITO extending out to the edge of the glass where external leads were connected. The thickness of the ITO was 150 nm. These ITO conductors are therefore unlikely to have significant effects on water diffusion at the glass/EVA interface.

The TiO_2 film was applied on top of the fork pattern in Figure 4.1 by delineating the area with adhesive tape and spreading Solaronix HT-L TiO_2 paste over the electrodes. The film was then sintered at 170°C for one hour. The resulting TiO_2 film was transparent. Film thicknesses varied slightly due to the manual production method, but were in the range 5 ± 3 μm, usually with approximately 2 μm of thickness variation across a given sensor film. For encapsulated calibration, sensors were laminated under a 0.5 mm thick EVA film with 33% vinyl- acetate content.

The measurement principle of the sensor is described in Publication I. Measured impedance curves were modeled with a resistance in parallel with a capacitive constant phase element. The ac-resistance R_{sensor} was determined by fitting the model to the measured data. Due to variations in resistance between individual sensors, it was convenient to define a resistance variable r as

$$r = \frac{\lg\left(R_{sensor}\right)}{\lg\left(R_0\right)}, \tag{4.1}$$

where lg (R_0) is the value obtained by extrapolating the lg (R_{sensor}) vs. RH curve, measured from the open sensor before encapsulation, to a relative humidity of 0%. This definition of r reduced the variation between sensors significantly.

4.1.2. Sensor calibration

The sensor developed here was calibrated both as an atmospheric humidity sensor open to the environment and as an encapsulated humidity sensor. The primary objective in both cases was to correlate the response r with the water mass concentration, c, in the TiO_2 film. This differs from the calibration of regular atmospheric humidity sensors. Water mass concentration in a film is more difficult to determine than atmospheric relative humidity. However, once its relationship to r is known, the calibration opens up a number of possible applications especially in the measurement of water mass transfer processes in encapsulated structures. Figure 4.2 shows the results of the atmospheric calibration measurement as an average calculated over 6 sensors. It is seen that the response r is very linear and independent of temperature.

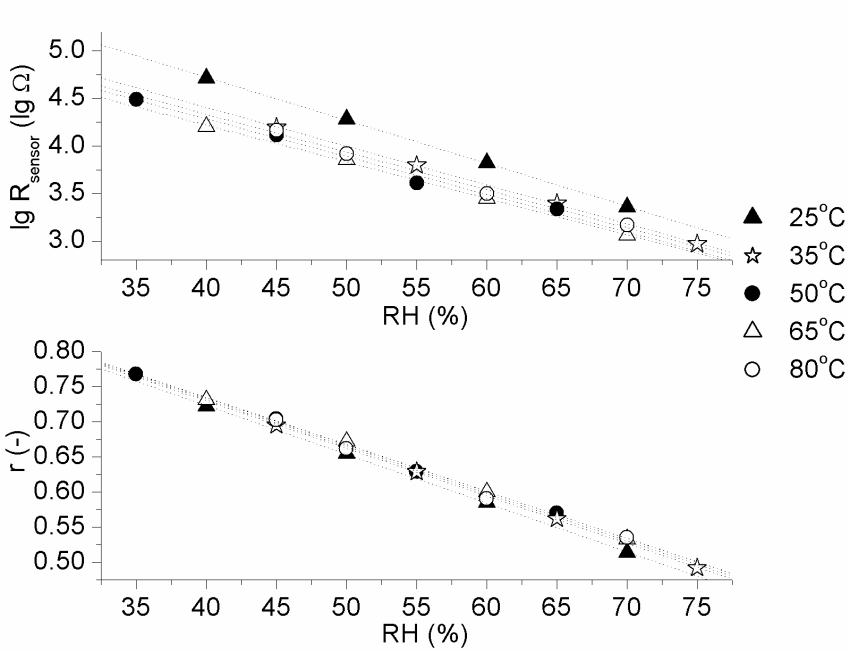

Figure 4.2: Results of atmospheric calibration measurement, average over 6 sensors. The response r is independent of temperature.

To calculate the r vs. c calibration curve from the data in Figure 4.2, it was necessary to correlate c with relative humidity. This was carried out with thermogravimetric experiments at room temperature, where the mass change during heating was taken to be equal to the adsorbed water within the TiO_2 pores. From the close correspondence of open sensor response with the Clausius-Clapeyron equation, it was further concluded

that the c(RH) function is independent of temperature, which allowed the calculation of the atmospheric calibration curve, yielding

$$r(c) = 1 - (5.4 \pm 1.7)\, c, \tag{4.2}$$

where c is expressed in mg per mm^3 of TiO_2 volume.

The encapsulated calibration was carried out with a water diffusion experiment where the sensor was laminated under an EVA layer and distilled water was allowed to diffuse through the EVA to the sensor. Figure 4.3 shows the experimental setup and defines the diffusion coordinate x, which is zero at the TiO_2/EVA interface. L is the EVA thickness, which was in the range 0.45 – 0.55 mm.

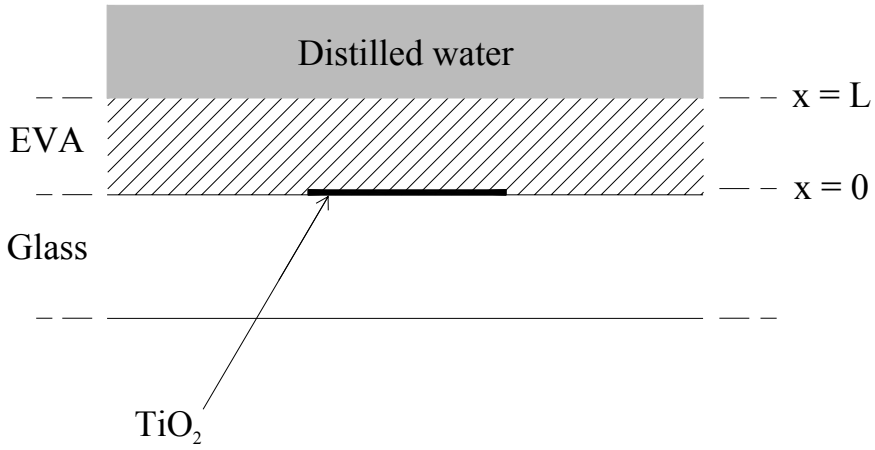

Figure 4.3: Experimental setup for encapsulated sensor calibration.

After the water had been poured on top of the sensor, its response was measured as a function of time. The water mass concentration within the sensor was calculated by modeling the diffusion process with Fick's law. The flux through the x = 0 interface, J_0, determined c through the equation

$$c(t) = \frac{\int_0^t J_0\, dt}{s} = \frac{\int_0^t -D \left.\frac{dC(t)}{dx}\right|_{x=0} dt}{s}, \tag{4.3}$$

where t is time, s is sensor thickness, D is the diffusion coefficient of water in EVA and C is the water concentration in the EVA. Taking the linearity of the atmospheric calibration curve as the starting point, the measured encapsulated calibration data was interpreted as evidence of three separate transport phases in the filling of the sensor. In phase number one, the sensor absorbed all the water which reached the x = 0 interface and J_0 was given by [88]

$$J_0(t) = -D \cdot \left.\frac{dC}{dx}\right|_{x=0} = \frac{DC_{sat}}{L}\left[1 + 2\sum_{n=1}^{\infty}(-1)^n \exp\left(\frac{-Dn^2\pi^2 t}{L^2}\right)\right], \quad (4.4)$$

where C_{sat} is the saturation concentration of water in EVA. In phase number two, the flux remained constant and in phase three it decreased linearly to zero as the sensor approached the limit where the TiO_2 pores were entirely filled with water. This model of the diffusion process was used to solve c(t) for three different sensors, all of which had a measured TiO_2 film thickness of approximately 3 μm. The r vs. c curves obtained through measurement of r(t) and modeling of c(t) for three separate sensors are shown in Figure 4.4. These are the encapsulated calibration curves for the sensors. Similarly to equation 4.2, an estimate for the encapsulated calibration curve can be written as

$$r(c) = (1.55 \pm 0.05) - (1.76 \pm 0.06)\, c, \quad (4.5)$$

where c is again expressed in mg/mm^3 of TiO_2 volume.

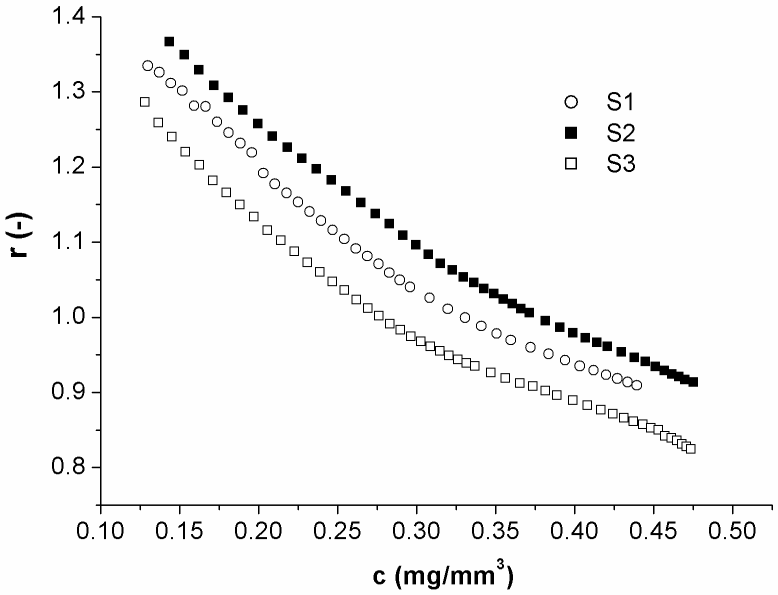

Figure 4.4: Encapsulated calibration curves for sensors S1, S2 and S3.

The uncertainty in the encapsulated calibration was larger than in the atmospheric calibration since there was a larger spread in the response from different sensors in the encapsulated experiments. The difference in the r vs. c slope between equations 4.2 and 4.5 indicates that the sensor has considerably greater sensitivity in atmospheric measurements. This can be explained by the fact that all of the water influencing the atmospheric measurement is adsorbed to the TiO_2 pore surfaces, whereas the value of c calculated in the encapsulated calibration experiment is likely to include both adsorbed and unadsorbed water. The first measurable signal in Figure 4.4 was obtained when approximately 10μg of water had entered the sensor. Based on the weather chamber calibration it is a plausible assumption that sensor response is independent of temperature in the encapsulated case as well. The sensitivity, transparency and

temperature-independent response of the sensor developed here indicate that this concept has the potential to be a useful tool in the characterization of water diffusion in PV module encapsulants.

4.1.3. Suggestions for improvements

The development of the sensor concept presented here is an initial inquiry into the possibility of measuring moisture with thin, porous films inside encapsulated test structures. Several interesting questions surrounding the sensor concept could not be explored due to lack of time and experimental resources. The following suggestions can be given for future work in this field:

1. *Alternative moisture sensor materials* could be explored. There is a great variety of thin, porous films which can be used to measure atmospheric humidity. As this thesis demonstrates, at least one of these, TiO_2, can be applied to moisture measurement when laminated under a polymer. Other metal oxides, such as Al_2O_3 or $MgAl_2O_4$, could be tested and their performance compared. Performance can be judged at least by sensitivity, linearity, stability, transparency, processing methods and compatibility with different conducting glass coatings or other substrates. A review of ceramic materials for humidity detection is given in [89].
2. *The stability of the sensor* is of great importance in accelerated aging testing. This aspect of the TiO_2 sensor was outside the scope of this thesis. In general, thermal stress at conventional PV module test temperatures is not expected to harm the TiO_2. A more important question is how the encapsulant/TiO_2 interface chemistry affects TiO_2 stability. UV-light in particular may cause photochemical reactions at the interface and the effect of photodegradation products, such as acetic acid in EVA, on the sensor needs to be clarified.
3. *Theoretical understanding* of the operational characteristics of the sensor could give interesting insights. A good basis for this exists in studies of atmospheric humidity sensors [89], but some aspects of laminated sensor impedance spectra, such as the elevation of Nyquist semicircles noted in Publication I, have not been observed in open sensors. In this context, it should be emphasized that measured values for the diffusion coefficient and saturation concentration of water in the polymer used for encapsulated calibration are needed for good precision. In this study, literature values were used in calibration.
4. *Precise processing methods* are important for preparing identical sensors. Preparation by hand, which was used in this thesis, inevitably leads to variations in film thickness and uniformity. It is also important to measure the thickness (or thickness profile) of the TiO_2 film with good accuracy before encapsulation, since the calculation of water mass concentration includes film thickness as one variable.
5. *New substrates and TCOs* could be explored to evaluate the utility of sensors structures in the study of flexible thin-film PV modules, for example. TCOs are an important factor in determining which materials can be used as moisture-sensitive films. Some TCOs are sensitive to high temperatures and require low-temperature processable films. The more durable TCOs are often more difficult to pattern, so many questions need to be explored to obtain the optimal solution. TCO thickness is also a variable parameter.

4.2. Sensor application: water absorption and desorption in EVA

(Publication II)

Some areas of investigation in which this sensor concept should be a useful tool were mentioned at the end of section 3.2.4. One of these is measurement of water absorption and desorption rates in laminated test samples with the same structure as real PV modules. Water penetration into PV modules is not a simple, unidirectional process where water always moves from the edges towards the middle of the module. Instead, the direction of water movement depends on the relation between module temperature and the temperature of the surroundings. If the module is at ambient temperature and is exposed to water, the water is absorbed by the module and diffuses inwards. But if the module is above ambient temperature, or if the surroundings are very dry, water will desorb from the module if a desorption path is available.

If the module has a glass/encapsulant/glass structure, the glass sheets can be considered impermeable to water and absorption/desorption will occur only at the edges of the module where the encapsulant is in contact with the environment. In modules with breathable back sheets both absorption and desorption will occur across a much greater area. The process will therefore be much quicker in breathable modules than in glass modules. Both module options entail a possibility of too much water exposure; in breathable modules because water will penetrate the module too easily, in sealed modules because any water which manages to penetrate through the sealant may stay inside the module even at high operation temperatures if the sealing prevents it from escaping.

With the development of the sensor described in this thesis, a diagnostic tool for evaluating different encapsulation options quantitatively is now available. By testing the absorption and desorption characteristics of different encapsulant materials and back sheets, the amount of water exposure a PV module would experience in the field can be measured and/or predicted if temperature and time of wetness data is available from field measurements. In Publication II, a study was conducted on the absorption and desorption characteristics of glass/EVA/glass laminates, the most common thin-film PV module configuration in use today. EVA is an interesting material to study because it has a relatively high water diffusion coefficient (10^{-7}–10^{-6} cm^2/s at 25^oC [67, 90]) compared to other possible PV module encapsulants. Whether this is a significant disadvantage or not depends on how quickly absorbed water can desorb from the module in high temperature conditions.

4.2.1. Sample structure and measurement principle

Water diffusion in encapsulant polymers at room temperature is a fairly slow process, and consequently the duration of an absorption experiment is quite long. In order to reduce the time needed for measurement, sensors were placed close to the edge of glass/EVA/glass laminates, as illustrated in Figure 4.5.

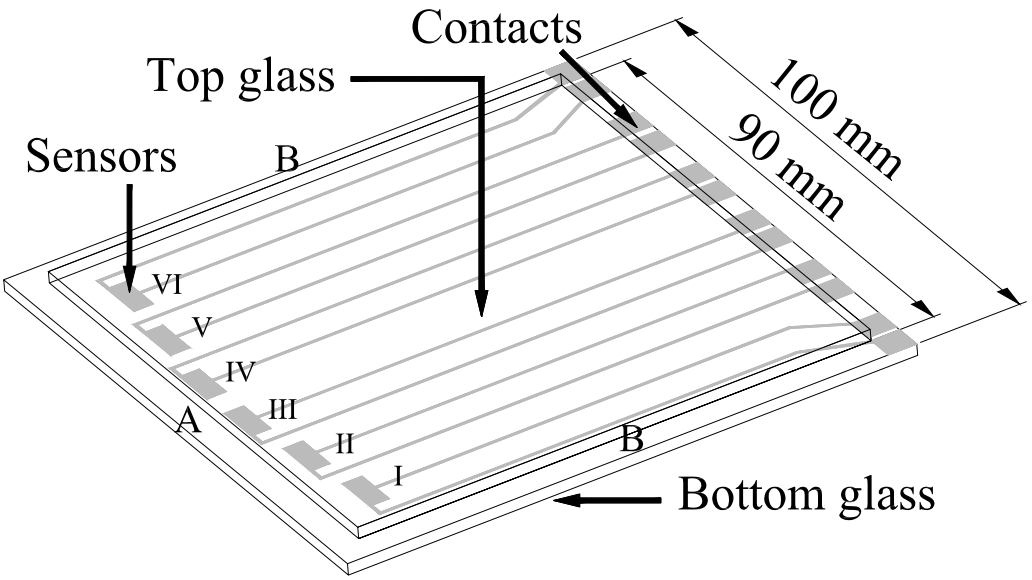

Figure 4.5: Glass/EVA/Glass laminate sample with sensors (I-VI) and contact areas for external leads indicated.

The gray area in Figure 4.5 shows the ITO-pattern on the bottom glass, with six separate interdigitated sensor electrodes, numbered I-VI. The top glass had to be smaller than the bottom glass to facilitate electrical contacting to the bottom glass at the indicated contact squares. During lamination, the top glass was kept in the right position with a copper frame and in the final laminate the distance of the edge of sensors III and IV from the top glass edge was approximately 2 mm. Sensors II and V were about 4 mm from the same edge and sensors I and VI 6mm from it. As the absorption experiments were carried out, sensors III and IV reacted several hundred hours earlier to water diffusion than the other sensors. The absorption/desorption experiments were therefore focused on sensors III and IV. The edges marked with B were sealed with silicone.

Water absorption rates were determined by placing the samples in an upright position in a bath of distilled water, with the contacts above water level. Desorption rates at sample temperatures of 35°C and 50°C were measured after the sample had been removed from the bath and placed on a hot plate at the chosen temperature. Desorption was measured at room temperature after removal from the water bath. PV modules in the field normally reach temperatures above 50°C for extended periods of time on sunny days, so both the desorption and absorption conditions corresponded approximately to those encountered outdoors.

4.2.2. Absorption and desorption results

Before absorption and desorption experiments were conducted, the behaviour of the sensor in desorption processes was studied. The possibility of water being locked inside the TiO_2 when the EVA dried out could not be ruled out without experimental evidence. For this purpose, absorption and desorption experiments were first conducted in a weather chamber with glass/EVA samples which reacted much more quickly to changes in the surrounding relative humidity than the glass/EVA/glass samples. By making a series of steps in chamber RH from a low value to a high value and back again, and by

logging sensor response during these changes, it was confirmed that the sensor reacts slightly more slowly to water desorption than to absorption. However, since this delay was on the order of minutes, it was insignificant in the desorption experiments described below where each experiment lasted several hours. The absorption/desorption experiments for the glass/EVA/glass laminates were conducted in sequential phases of absorption and desorption to study the effect of multiple cycles on the water absorption rate. Figure 4.6 shows the time series for two laminate samples, S1 and S2. To illustrate how high the measured R_{sensor} values were, the axis on the right shows the lg R_{sensor} values of sample S1 corresponding to the value of r on the left axis.

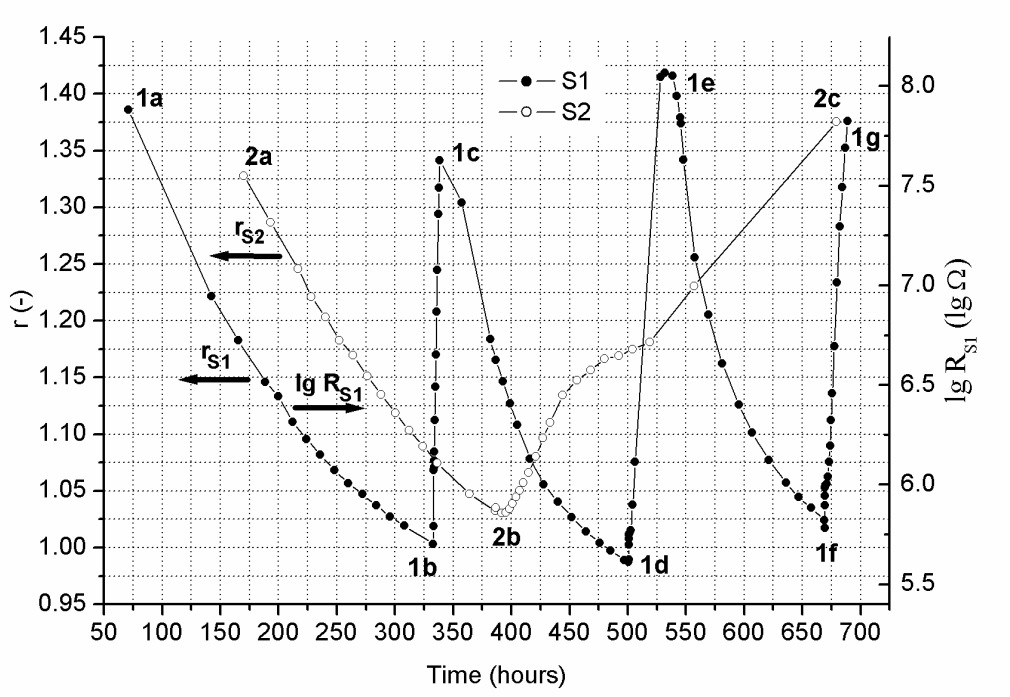

Figure 4.6: Measurement results from sequential absorption/desorption experiments for two glass/EVA/glass laminate samples.

It is seen that the sensor in S2 reacted significantly later to the incoming water than the sensor in S1 during the first absorption phase. This is due to a difference in the distance from the sensor edge to the top glass edge between these two sensors. In this study, the absorption and desorption rates were evaluated by comparing the time needed for the sensor to change from a response of approximately r = 1.35 to a response of r = 1.05 (or, in the case of desorption, to undergo the opposite change). This was the most convenient method because the sensor does not give a signal when the EVA is completely dry, so no method would have been available for confirming when the EVA had dried out in a desorption experiment. This would have made it difficult to know when the next absorption phase should have been started. It is also worth noting that the situation in a real PV module deployed in the field is often one where some water is still present in the EVA when a new diffusion front begins to penetrate the module.

Each absorption phase in Figure 4.6 was performed at room temperature, as was the desorption phase for sample S2. For sample S1 the desorption phases were conducted at 50°C (1b–1c) and 35°C (1d–1e and 1f–1g). A comparison of absorption and desorption rates can be made by plotting the different parts of Figure 4.6 with suitable adjustments

along the time axis. Figure 4.7 shows the three absorption phases of sample S1 with a common starting point indicated by the letter a.

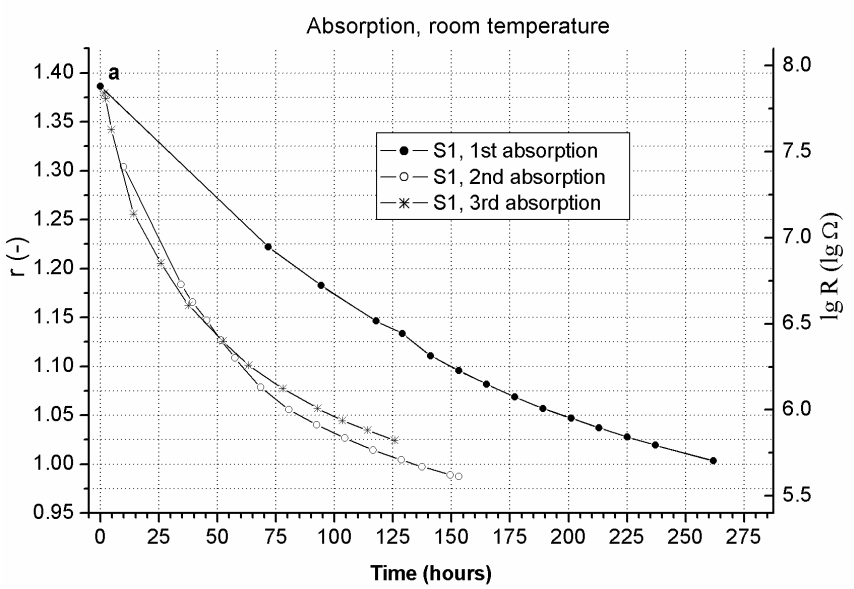

Figure 4.7: Comparison between the first, second and third absorptions in sample S1.

It can be seen that water absorption proceeded significantly quicker the second time than it did in the first absorption, but the third absorption developed approximately at the same rate as the second one. This indicates that completely dry EVA resists moisture better than once wetted EVA. The first and third desorptions from sample S1 and the one desorption from sample S2 are plotted in detail in Figure 4.8, with t = 0 indicating the moment when the sample was removed from the water bath.

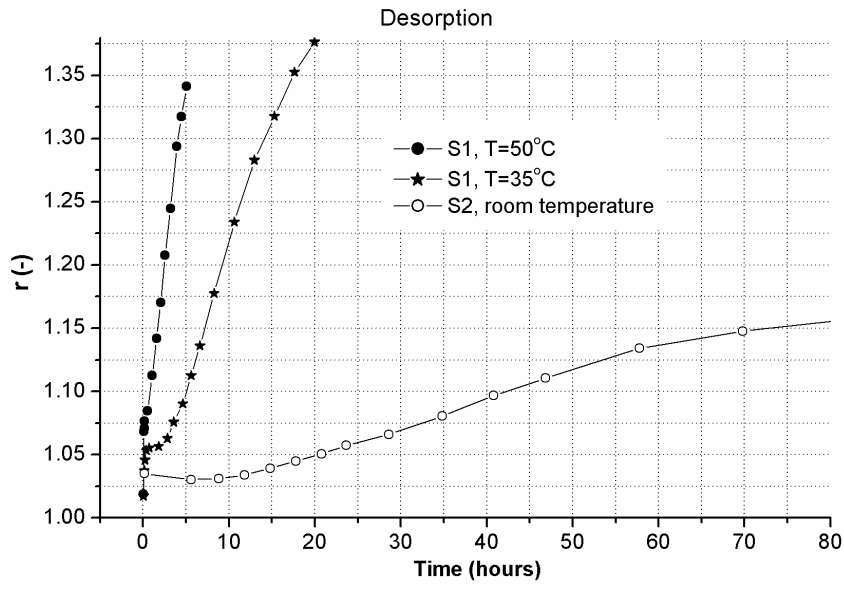

Figure 4.8: Comparison of the desorption measurements from samples S1 and S2.

Although the difference in distance to edge brings some uncertainty to the comparison between S1 and S2 in Figure 4.8, it can still be seen that the influence of sample temperature on the desorption rate was very significant. Room temperature desorption proceeded approximately at the same rate as absorption, whereas the S1 sample dried out in approximately 20 hours at 35°C and in 5 hours at 50°C. The approximate times needed for the r = 1.05 → 1.35 or r = 1.35 → 1.05 transition in the cases presented above is shown in Table 4.1 below.

Table 4.1: Comparison of absorption times for 1st, 2nd and 3rd absorptions in sample S1, and for desorption times at different temperatures in samples S1 and S2.

#	Absorption	T_{sample}	Desorption
1st	182 h (S1)	room	260 h (S2)
2nd	81 h (S1)	35°C	20 h (S1)
3rd	95 h (S1)	50°C	5 h (S1)

Desorption at 50°C was thus estimated to be about 16 times quicker than absorption at ambient temperature and at 35°C the desorption rate was still fourfold compared to the absorption rate. With these desorption rates, it seems likely that unframed PV modules encapsulated with EVA will dry out significantly during the summer in most climates. The seasons when there is so little sunshine that modules do not experience temperatures above ambient for long periods of time may be more critical for module stability. Such conditions are quite common in the winter climates of North and Central European locations. It is worth pointing out that the EVA studied in this work did not undergo thermal or UV-stress during the experiments. The effect of encapsulant polymer aging on its water absorption and desorption characteristics should be investigated in future encapsulation studies.

The question of how a module should be encapsulated to minimize water exposure is a complex one. An encapsulation polymer with a very low diffusion coefficient may limit the alternating penetration and escape of water to a small area at the module edge, but water escape may also be significantly slower from such a polymer than from EVA. The design of the PV module edge is an important aspect of its moisture stability, especially with regard to how moisture-induced damage at the edge of the module influences its operation. In general, it is a fundamental objective in PV module design to maximize the active area, so a very wide inactive safety zone at the edge of the module is usually not an attractive option. Different sealing alternatives and breathable back sheets add additional complexity to the problem. The maximization of PV module moisture resistance is thus influenced by a multitude of factors which have to be optimized to achieve high performance at an affordable price. The sensor concept described in this chapter is a useful tool for comparing the different alternatives, and it can probably be applied also in field testing. However, factors affecting sensor stability should be investigated prior to field experiments.

5. Analysis of field-tested thin-film PV modules

(Publications III, IV, V, VI)

Field testing of PV modules is the most reliable method for verifying stability. If modules do not show any signs of degradation after long-term operation outdoors, they can be considered stable in the climate where the tests were performed. However, there are several reasons why field tests are not by themselves sufficient for reliable stability studies. Some of them have to do with practical feasibility, while others are concerned with accuracy. From the perspective of this thesis, the ones of greatest importance are the following:

1. To confirm a module lifetime of 20 or 30 years the field tests, in principle, need to last equally long. Even if some uncertainty is accepted, test periods need to be at least 5 years long to cover the expected initiation time for the most common degradation mechanisms and to ensure that the modules are exposed to all relevant weather conditions. This is a long time to wait for test results since product improvement usually develops in much shorter cycles.
2. Field tested PV modules are tested in their final, encapsulated state. When performance degradation is observed, it is in most cases difficult to attribute it to any specific degradation mechanisms or to locate it in a specific cell, because the measurements only reveal the operational characteristics of the entire module.
3. In field tests, modules are exposed to a great variety of weather conditions. This reduces the accuracy of field test data analysis since variations in meteorological variables cause uncertainty in the measured data. This problem can be avoided by periodic removal and simulator-measurement, but this is seldom possible when full-size modules are tested.
4. Results obtained at one testsite are not necessarily reliable indicators of stability in other locations. Field testing needs to be conducted in a number of different climates to gain certainty in stability estimates. However, extensive international testing is usually prohibitively expensive.

This work presents new methods for mitigating these problems in field testing of thin-film PV modules. All field test measurements reported here were conducted at the Helsinki University of Technology (HUT) solar energy testsite (location N 60°11', E 24°49'). The data on CdTe and CIGS modules was collected as a part of the EU project PYTHAGORAS, details of which are presented in Publication VI. The studied modules were commercially available, 60cm x 120cm in size. Field tests lasted from the summer of 2001 to the end of 2003. During this time, 16 CdTe and 16 CIGS modules were under continuous measurement. Figure 5.1 shows the complete installation of 32 modules, oriented southwards and tilted at an angle of 45°, at the HUT testsite. The IV-curves of all modules were logged separately through the electronic loads illustrated in Figure 5.2. Module temperatures (T_{mod}) were measured continuously from three modules of each technology. Measured meteorological variables included plane-of-array irradiance (G), global horizontal irradiance (G_H), diffuse horizontal irradiance (G_D), ambient temperature (T_{amb}) and wind speed. Details on the Pythagoras project are presented in Publication VI and further information on the measurement methodology is available in [91]. As presented in Publication VI, the efficiency of the modules tested in the latter part of the project was stable and no immediate indications of degradation were observed. These results do not include the CdTe modules tested at the beginning of the project, which did degrade in outdoor use. An analysis of the degradation

observed in the CdTe modules is presented in Publication III and discussed in detail below.

Figure 5.1: 32 CdTe and CIGS modules under measurement at the HUT testsite in July 2002.

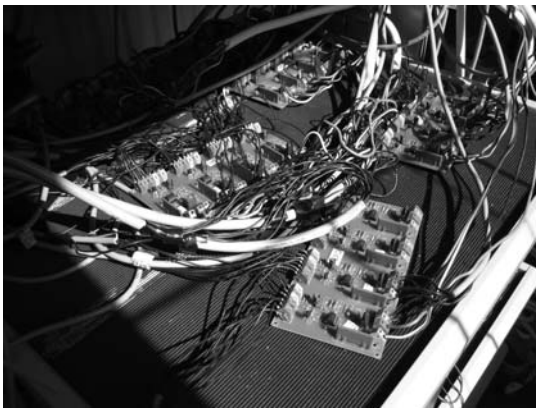

Figure 5.2: Module connections to circuit boards with electronic loads.

The field test data for BIPV single-junction a-Si modules analyzed in this work was measured in the EU project ASICOM [92] at the Helsinki University of Technology solar energy testsite from 1998 to 2001. Figure 5.3 shows the vertical, southwards oriented BIPV facade with 18 a-Si modules integrated to a wooden container. The measured parameters included the total power of 6 three-module systems and the meteorological parameters G and T_{amb}. T_{mod} was also measured from several locations in the facade. Temperature data from four triple-junction a-Si PV modules integrated to a free-standing roof, shown in Figure 5.4 and tilted 45^{o} southwards, was used as a comparison to the BIPV case. The data measured from these modules was obtained at the testsite between 2002 and 2004 and it included G and T_{mod} values as well as module IV-curves. Further details on the a-Si measurements are given in Publication V.

Figure 5.3: a-Si BIPV facade at the HUT testsite, with 18 modules.

Figure 5.4: Four a-Si modules integrated to a free-standing roof at the HUT testsite.

5.1. Degradation analysis of field-tested CdTe modules

(Publication III)

In the first phase of the PYTHAGORAS field test project, results from the HUT testsite showed that the performance of the CdTe modules degraded during the first year of outdoor operation. The mechanisms behind performance loss were investigated in Publication III with a study of small-area samples from the full-size modules. Figure 5.5 shows the relative degradation observed (at G = 800 W/m^2) in two modules, F1 and F2, which were chosen for sampling, and the average degradation of all 16 modules. It is seen that the degradation in P_{MPP} is primarily explained by a large fill factor loss, and a drop in V_{OC} is also evident. The loss of power in module F2 is approximately equal to the average loss, while F1 degraded slightly less.

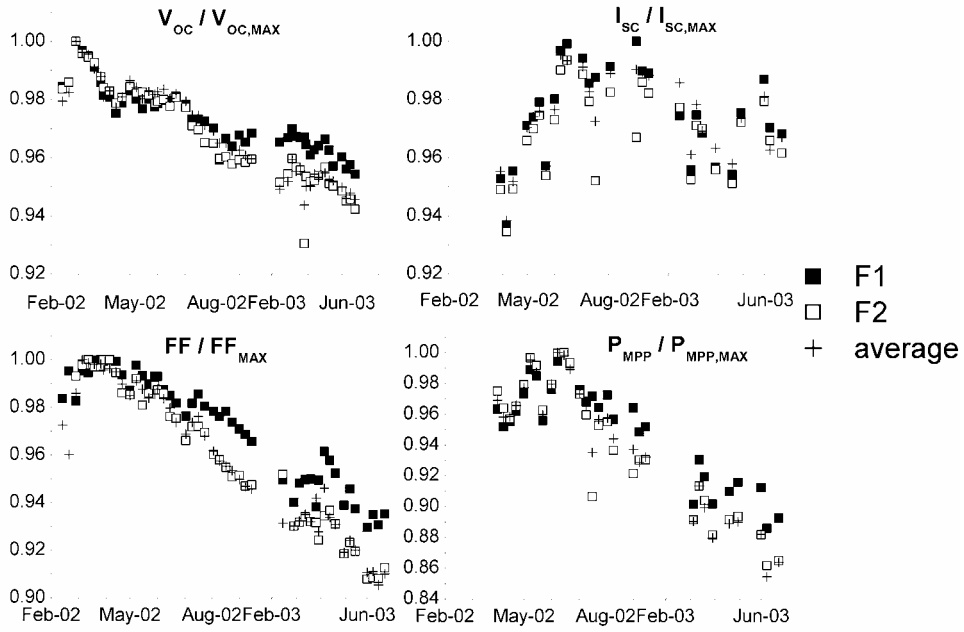

Figure 5.5: Performance loss in CdTe modules during 1½ years of outdoor exposure in Finland. Modules F1 and F2 were sampled.

As stated earlier, a primary problem in field testing is that it is difficult to uncover the degradation mechanisms behind performance loss. In some cases visual inspection may point directly to a given mechanism, for example if corrosion, encapsulant coloring or delamination (air bubbles) can be clearly seen. However, visual inspection is difficult to quantify and many degradation effects do not manifest themselves in a visible manner. A more detailed understanding of degradation may sometimes be gained by using specially designed modules which allow in situ measurements from several different contacts within the module. In other cases, selective shading of the module may be a useful diagnostic tool. A fourth option, which was employed in this thesis, is de-encapsulation of the module to reveal the open cell surface on which electrical or microscopic studies can be conducted.

5.1.1. De-encapsulation and sample preparation

Sampling based on de-encapsulation of PV modules contains uncertainties related to maintaining the samples in their original state during the removal of the surrounding glass and encapsulant. An especially important problem is exposure to liquids, because lubricants are usually needed in glass cutting and polishing. In this study, nine glass/CdTe/encapsulant/glass samples about 20·25mm in size were cut with a tile cutter from modules F1, F2 and a reference module (labelled REF) which had not been used outdoors. It is unlikely that the water used for lubricating the cutting affected the samples in this workphase, since the cutting was a quick process (3-4 minutes per sample) and the cell area which was later characterized lay in the center of the sample.

In the second de-encapsulation phase the backside glass was polished away on a water-lubricated SiC grinding pad. Polishing was stopped after approximately 10 minutes, when a very thin layer of backside glass remained on the sample. The sample was then dried in warm air and the remaining glass was peeled off by hand, followed by peeling of the encapsulation film. It is not likely that water could have reached the center of the sample as long as a significant thickness of backside glass remained, but some water exposure inevitably occurred in the finishing stage just before the mechanical polishing was stopped. However, it is unlikely that the samples suffered from this exposure, since they remained protected by the encapsulation film, the exposure lasted only a few minutes and they were dried in warm air immediately when the remaining glass was judged to be sufficiently thin. Upon removal of the encapsulation film the sample surface was always found to be clean and dry in optical microscope inspection. A few samples cracked during polishing. The number of studied samples was thereby reduced to 6 for modules F1 and F2, and to 7 for REF.

For electrical characterization, samples were contacted according to the scheme presented in Figure 5.6 by applying silver paint to the striped areas.

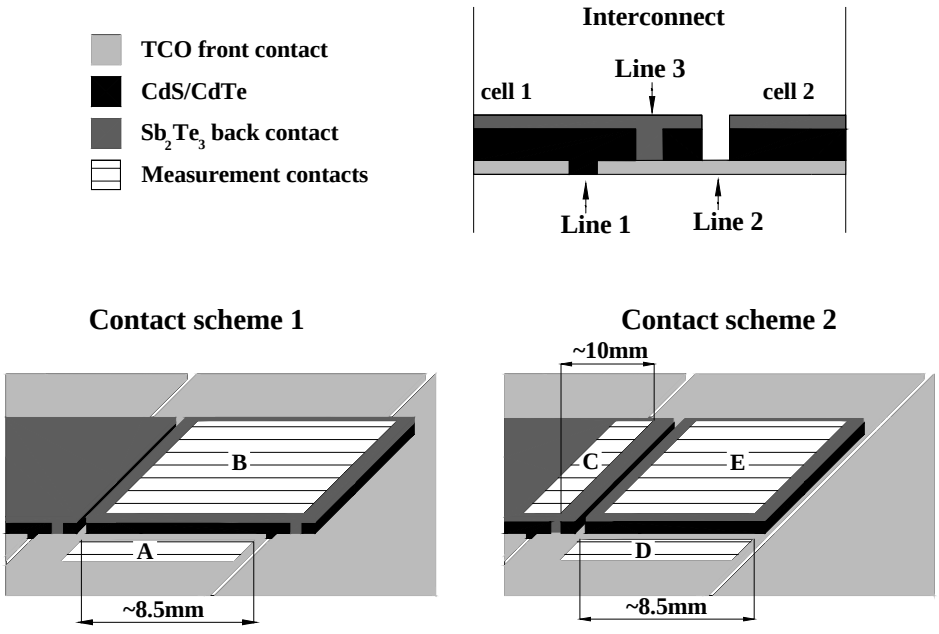

Figure 5.6: Two contacting schemes for CdTe module samples, and a closer view of the interconnect structure.

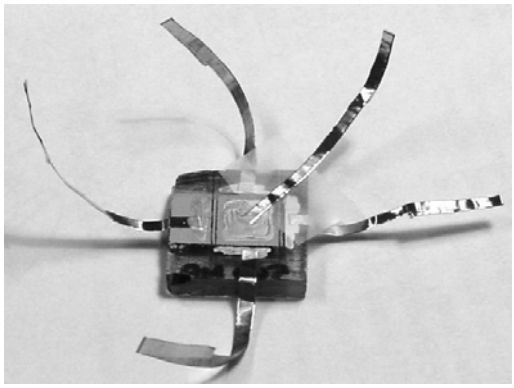

Figure 5.7: A contacted CdTe module sample.

The basic objective of the characterization was to separate interconnect degradation from cell degradation. The interconnect degradation modes were evaluated as resistive changes through their impact on the measured sample IV-curve. These degradation modes included increased shunting between front contacts at scribe line 1 of the interconnect region (degradation mode D_{SH}) and increased series resistance at lines 2 or 3 ($D_{TCO/back}$). Other degradation modes included resistance increase in the front and back contacts (D_{TCO} and D_{back}) and performance loss in the active materials (D_{cell}).

Table 5.1 shows which degradation modes were included when measurements were conducted from a given pair of contacts in Figure 5.6. A photograph of a contacted sample is shown in Figure 5.7, with copper tape strips connected to all measurement locations. Contacting and characterization was first done with scheme 1, then the area crossing the interconnect was removed with a scalpel and the sample was recontacted and measured from the scheme 2 contacts. During silver paint contacting the cell area was protected from shunting with adhesive tape. Samples were cleaned with acetone between the two contacting phases.

Table 5.1: Degradation modes affecting the measurement from different contacts.

Contacts	Degradation modes
A-B	D_{TCO}, D_{cell} and D_{SH}
C-E	D_{TCO}, D_{cell} and $D_{TCO/back}$
D-E	D_{TCO} and D_{cell}

5.1.2. Sample characterization results

Measurements were conducted separately for all three contacting alternatives presented in Table 5.1. It was observed that the average IV-curves measured with contacts A-B, C-E and D-E were nearly identical for each module except for a lesser rollover in the A-B measurement at voltages higher than V_{OC}. Since the curves were identical in the fourth quadrant, it was concluded that degradation modes D_{SH} and $D_{TCO/back}$ did not contribute to degradation. The degradation mechanisms were therefore sought through a closer analysis of the IV-curves measured from contacts D-E.

Figure 5.8 shows the first and fourth quadrant data for the average D-E IV-curves of F1, F2 and REF. Table 5.2 presents the corresponding performance parameters. The most notable differences are in I_{SC} and FF and in the much lesser rollover at far forward bias for module F1. As will be discussed in the next section, differences in I_{SC} cannot be directly interpreted as an I_{SC} difference between the full-size modules, because currents

are lower in large modules. However, the FF difference is likely to be a relevant indicator of the outdoor degradation presented in Figure 5.5.

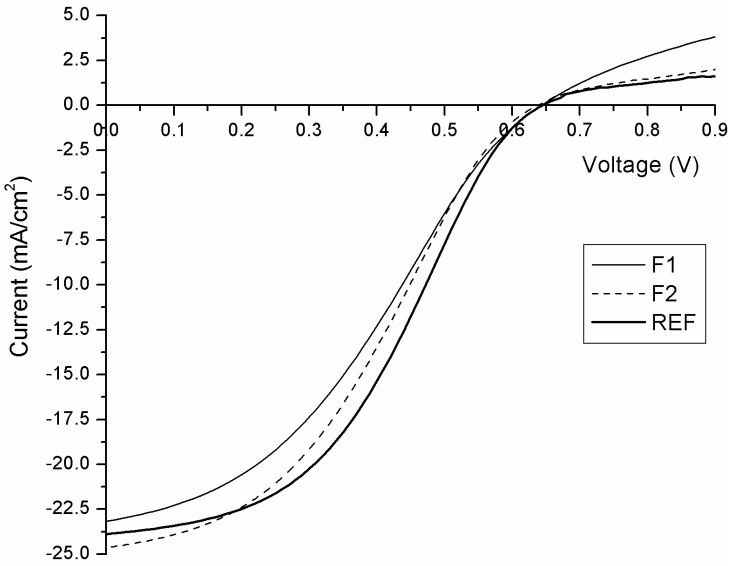

Figure 5.8: Comparison between the average sample IV-curves for modules F1, F2 and REF.

Table 5.2: Performance parameters from Figure 5.8.

Module	I_{SC} (mA/cm^2)	V_{OC} (V)	FF (%)
F1	22.2	0.63	37.5
F2	24.1	0.62	39.0
REF	23.9	0.64	41.3

The degradation was analyzed further by evaluating the shunt conductance from the measured IV-curves at far reverse bias. It was observed that dI/dV was consistently about 50% higher for F1 and F2 than for REF, which indicated that there was a greater degree of shunting in the cell material of modules F1 and F2 than in REF.

Since TCO resistance may also have contributed to the FF degradation seen in modules F1 and F2 in Figure 5.8, the resistance between two contacts on opposite sides of the active material, such as the uppermost and lowermost contacts in Figure 5.7, was measured. The average resistance in samples from modules F1 and F2 was 6% and 9% higher than the average resistance in REF samples. However, the validity of this result was uncertain due to large variations between samples.

Finally, capacitance-voltage measurements were used to compare the apparent doping concentration profiles of the samples. Figure 5.9 shows the calculated average doping profiles for samples from each module. It is seen that the profiles of F2 and REF were nearly identical, but that the depletion region of the F1 module was significantly wider. Combined with the reduction of rollover observed in Figure 5.8, the outdoor

degradation of module F2 bears a close resemblance to the degradation reported from accelerated aging tests on CdTe cells with similar back contacts in [26]. The transport of dopants away from the junction, seen in Figure 5.9, is likely to reduce the collection efficiency of the solar cell, since the electric field becomes weaker and more charge carriers recombine before they cross the junction. If the dopants accumulate close to the back contact, this may produce the reduction in rollover observed in this study and in [26]. The increased shunting in the cell was most likely due to a separate degradation mechanism since no significant difference between F1 and F2 was observed in this respect.

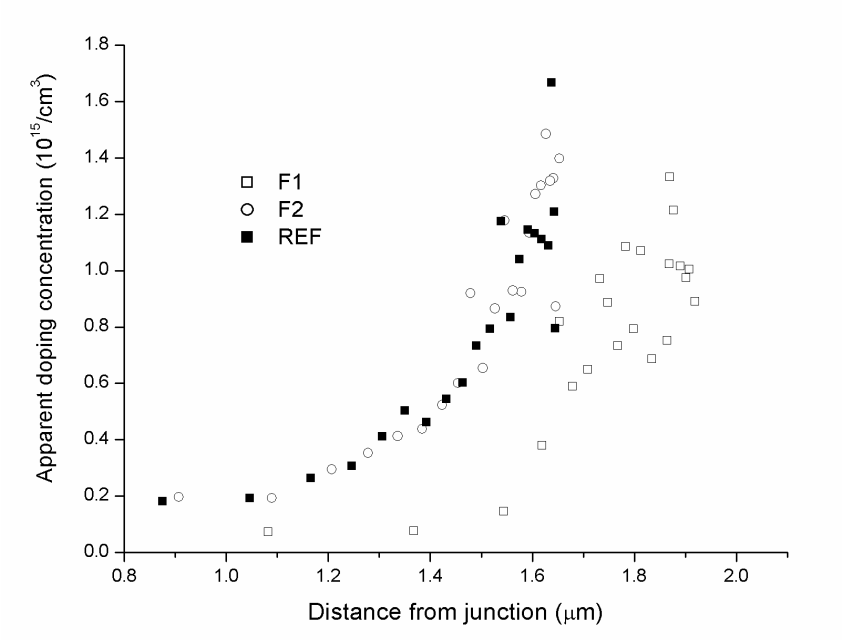

Figure 5.9: Apparent doping concentration profiles for samples from the three modules.

In summary, three degradation mechanisms (dopant transport away from the junction, increased TCO resistance and increased shunting within the cell) were observed, and they appear to be independent of each other. Evaluating the relative importance of each degradation mechanism is a complex task, especially since the connection between sample results and large module degradation is not a one-to-one relationship.

5.1.3. Interpretation of module degradation from small sample results

In a large thin-film PV module, several factors combine to make the module efficiency lower than the efficiency of single cells. This was an important issue in this study, because the question of whether the 1cm^2 samples studied in this work give an accurate picture of 60 x 120 cm^2 module degradation is crucial. It is possible that some of the degradation mechanisms found in the small sample studies were irrelevant in module degradation and that degradation in the field was instead caused by mechanisms which manifest themselves only over a large area or at the edges of the module. To clarify this issue, the IV-curve of the entire module F1 measured in the field early in the test period was compared to the simulator-measured IV-curve of a 1cm^2 sample taken from module REF, which was representative of the average behaviour of an undegraded small sample. The field measurement in question had been recorded at an irradiance very

close to the standard simulator irradiance of 1000 W/m^2. The IV-curve of the large module was rendered comparable to the curve of the small sample by dividing module voltage with the number of individual cells and by dividing module current with the area of one cell. In the comparison it was observed that the short-circuit current density of the large module was only 66% of that measured from the small REF sample, the average V_{OC} per cell in F1 was 95% of the V_{OC} measured from the sample and the FF of F1 was 6% (relative percentages) higher than that of the sample.

The current density of a large module is usually less than a single cell can produce due to current mismatch between the individual cells of the module, non-uniformity within cells and resistive losses. In this study, the current of F1 was found to be so much smaller than the current obtained from the REF module sample that it would not have been possible to interpret degradation in small sample current as a reason for module current loss. Module voltage is calculated as a sum of 'weakest links', since the voltage of each cell in the module is as high as its weakest point allows it to be. The difference between module and small sample voltages was approximately of the same size as the degradation observed in the field, so a definite conclusion regarding module voltage degradation could not be drawn from sample studies either.

However, FF degradation in small samples is in most cases a good indicator of FF decrease in the module. The fill factor is determined by series and shunt resistance and by the diode characteristics of the cell material. Severe shunting in one small area of the cell would reduce its FF, but this shunt would also give a much lower V_{OC}. In the absence of shunts the cell FF is not severely affected by a highly localized increase in resistance or a local worsening of the diode characteristics. This is because alternative current transport routes are usually available, so a very resistive path can be avoided. Similarly, a worse diode structure in a limited region does not harm the operation of the cell in other regions. The small sample results in this study attributed FF degradation to a slight increase in TCO resistance and to a changed doping profile in one of the modules. These factors most likely played a part in module FF degradation, but the possibility that other mechanisms also contributed could not be ruled out.

It is worth noting that the number of studied samples has important implications for the conclusions which can be drawn from small sample studies. If current degradation is studied, a very large number of samples would have to be gathered and all individual cells should be included. This is not a practically feasible method. Optoelectronic measurements, such as laser-scanning which does not require de-encapsulation, are a more useful tool for these investigations [17]. Studies of module voltage degradation through small-sample analysis also require a large number of samples, since local shunts may act to degrade module voltage without affecting other areas of the cell. For fill factor studies the situation is different. In the absence of severe shunting, an increase in resistance or changes in the diode will affect the FF of the cell and the module only if they occur over a larger area. FF degradation can therefore be monitored with a smaller amount of samples than I_{SC} and V_{OC} degradation. However, the degradation studies conducted in this thesis would probably have needed a larger number of samples to produce precise information and rank ordering of degradation mechanisms. Unfortunately, the number of samples had to be limited due to practical considerations and was further reduced by breakage in the sample preparation process.

5.2. Improving field test analysis through data filtering

(Publication IV)

The third problem with field testing, as stated at the beginning of this chapter, is that test conditions are not stable. Cloudiness, wind speed at the module surface and momentary solar spectrum are only a few of the factors which contribute to uncertainty in field test measurements. This makes it difficult to detect small changes in module performance because they may be hidden by changes in meteorological parameters. The solution to this problem is obvious: to measure as many meteorological parameters as possible and to restrict the analysis to a given range of values. If the chosen parameters and value filters are good, the data will contain much less uncontrolled variation. This logic is applied in all field data analyses, at the very least by selecting a certain plane-of-array irradiance range within which the analysis is carried out. However, the rationale behind the selection of filtering criteria is rarely stated explicitly. Choices are usually made based on educated guesses or assumptions.

In Publication IV, an analytical method was developed for evaluating the effect that different filtering criteria have on the accuracy of performance parameter evaluation and on the number of data points which remain after filtering. The method allows a close tracking of changes in module performance parameters and thereby makes it easier to observe degradation.

5.2.1. Utility comparisons for filtering criteria

In the study conducted in Publication IV, CIGS module field test data collected between April and October 2002 was used to study the effect of data filtering on analysis accuracy. Table 5.3 shows the measured variables which were used in the filtering, and the criteria which were imposed on their values. By choosing one criterion from each row and filtering the original data set with this combination of criteria, a new, filtered data set was created. For each irradiance level, a total of 5184 of these filtered data sets were created and evaluated. For notational clarity, the symbol Ω was used as a variable referring to any combination of filtering criteria from Table 5.3.

The purpose of the study was to develop a methodology for evaluating the utility of the data set created by each Ω in two respects: **a)** the precision of the daily value of a given performance parameter Y (the variable Y refers to I_{SC}, V_{OC}, FF or P_{MPP}) in the data set should be high, and **b)** the number of days from which a value is available should be high. It is evident that these demands are in conflict, since a strict filtering will yield data from well-defined weather conditions but the number of days when these conditions occur will be small. Conversely, the number of days is large if nearly all conditions are accepted, but a lot of variance will then be present in the data.

Two common ways of reducing scattering in field data is to calculate linear temperature corrections to measured current and voltage variables and to assume a linear relationship between G and the current variables I_{SC} and I_{MPP}. This is a straightforward procedure because these relations are usually very linear. These corrections were utilized in this study as well. Irradiance corrections could be implemented directly in the raw data. Temperature corrections were carried out by first conducting an initial comparison of the filtering criteria in Table 5.3 based on Ω(ΔG, R_{min}, θ_{min} and θ_{max}) but without any module temperature restrictions. The data set created by the best one of

these Ω was used to calculate temperature coefficients for the relevant performance parameters. When the coefficients had been calculated, temperature corrections were applied to all measured performance parameters in the full, unfiltered data set. A second filtering run was then conducted with Ω(ΔG, T_{min}, T_{max}, R_{min}, θ_{min} and θ_{max}).

Table 5.3: The filtering parameters and the criteria imposed on them.

Filtering parameters	**Filtering criterion**	**Criteria per G_0**
Irradiance level (G_0) and width of irradiance interval (ΔG)	$\mathbf{G_0 - \Delta G/2 < G < G_0 + \Delta G/2}$ with G_0 = 400, 600, 800, 1000 W/m^2 and ΔG = 60, 80, 100 W/m^2	**3**
Module temperature minimum (T_{min}) and maximum (T_{max})	$\mathbf{T_{min} < T_{mod} < T_{max}}$ with T_{min} = 10,20,30 ... 60°C and $T_{max} = T_{min}$+10°C, T_{min}+20°C, T_{min}+30°C	**6** **3**
Minimum of G_H/G_D ratio (R_{min})	$\mathbf{R > R_{min}}$ with R_{min} = 1, 2, 3 ... 8	**8**
Minimum (θ_{min}) and maximum (θ_{max}) angle of incidence	$\mathbf{\theta_{min} < \theta < \theta_{max}}$ with θ_{min} = 0, 10, 20 ... 50° and $\theta_{max} = \theta_{min}$ + 20°, θ_{min} + 30°	**6** **2**
		Π 5,184

The utility comparison between different Ω was carried out by calculating the average daily standard deviation, $\overline{\sigma_Y}$ (Ω), for measurements of a performance parameter Y in the filtered data set. A daily standard deviation of Y measured from one module was calculated only if three or more IV-scans were available from that module on the day in question. The value $\overline{\sigma_Y}$ (Ω) was calculated as the average of the standard deviation in Y over all days with at least 8 modules included in the averaging. Finally, the ratio f(Ω) between the number of days with measurement data and the total number of days in the measurement period was calculated.

The conditions a) and b) referred to at the beginning of this section could be formally stated as a) $\overline{\sigma_Y}$ (Ω) should be as small as possible and b) f(Ω) should be as large as possible. A plot of f(Ω) versus $\overline{\sigma_Y}$ (Ω) shows the information needed for selection of the best combination of filtering criteria. Figure 5.10 shows this plot for the temperature-corrected values of V_{OC}, FF, I_{SC}/G and P_{MPP}/G at irradiance G_0 = 400 and 600 W/m^2. The circled points at 600 W/m^2 indicate the Ω chosen as the best ones. This choice is to some extent subjective, since several different Ω often cluster in the same area and are equally good. For FF, the $\overline{\sigma_Y}$ values with f > 20% are smaller than the error estimate, which prohibits the analysis of FF variation at this irradiance.

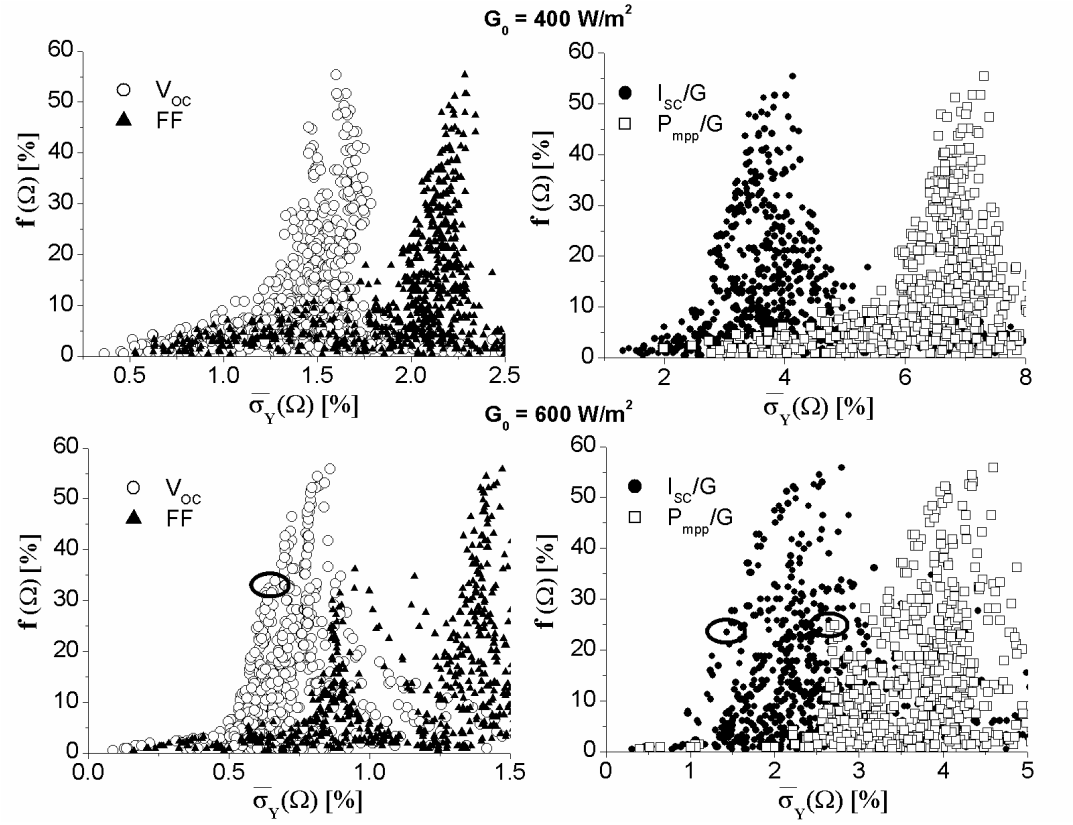

Figure 5.10: f(Ω) versus $\overline{\sigma_Y}$ (Ω) for temperature-corrected data at 400 and 600 W/m^2. The circled points at 600 W/m^2 indicate the criteria chosen as the best ones in this study.

In Figure 5.11 the same data is shown for G_0 = 800 and 1000 W/m^2. The obtainable $\overline{\sigma_Y}$ values decrease significantly with increasing irradiance for all performance parameters. This illustrates that sunny conditions are always the best conditions for performance monitoring, but it should be remembered that low-irradiance performance is often a separate point of interest, and analyses where it is sought need particularly good data filtering. As for FF above, the standard deviations of FF and P_{MPP}/G in Figure 5.11 are smaller than the estimated measurement error for these parameters. The inaccuracy in FF and P_{MPP} determination is caused by the low number of points on the IV-measurement curve. For V_{OC} and I_{SC} / G, the points corresponding to the best Ω have been circled in Figure 5.11.

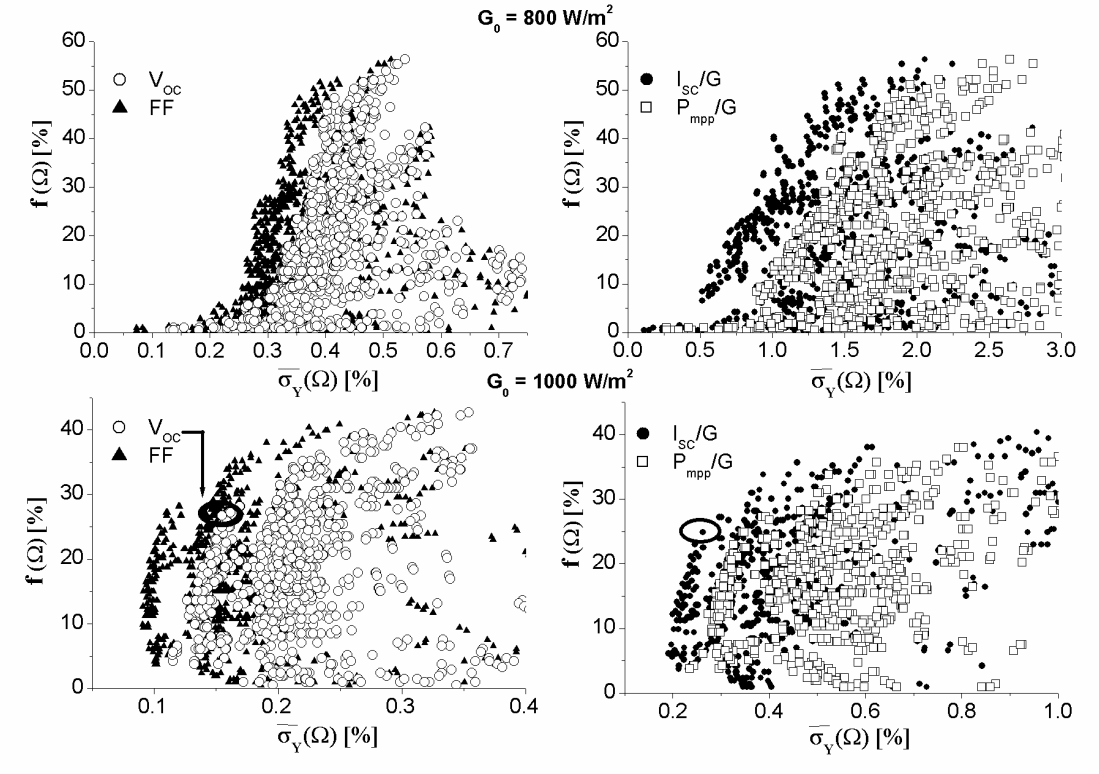

Figure 5.11: f(Ω) versus $\overline{\sigma_Y}$ (Ω) plots for temperature-corrected data at 800 and 1000 W/m^2. The circled points at 1000 W/m^2 indicate the criteria chosen as the best ones in this study.

5.2.2. Estimation of accuracy gain in data filtering

To illustrate the benefit of finding appropriate filtering conditions before an analysis of field test data is performed, a comparison was performed by analyzing the field test data studied in this work in two separate ways: A) by filtering the data with the criteria corresponding to the circled points in Figures 5.10 and 5.11 and B) by a simpler method, where an irradiance interval was selected and temperature corrections were calculated, but no additional filtering was performed. Figure 5.12 shows the resulting time series for P_{MPP}, V_{OC} and I_{SC} at 600 W/m^2, and for V_{OC} and I_{SC} at 1000 W/m^2, obtained with these two methods. It is clear that filtering the data reduced scattering and the accuracy gained by filtering was particularly marked at 600 W/m^2. Calculations show that the filtering method employed here reduced the residual variance in the data by 61–73% for the parameters evaluated at 600 W/m^2 and by 40% and 79% for V_{OC} and I_{SC} at 1000 W/m^2, respectively. The number of days with measurement points was reduced by 54–58% at 600 W/m^2 and by 46% at 1000 W/m^2.

It is evident that data filtering is particularly valuable at low irradiance, because there's much more variation in meteorological parameters in these conditions. Filtering also helps especially in the analysis of module current and power, since the current is very sensitive to both the intensity and the spectral distribution of sunlight. Voltage can be studied fairly accurately even without detailed data filtering.

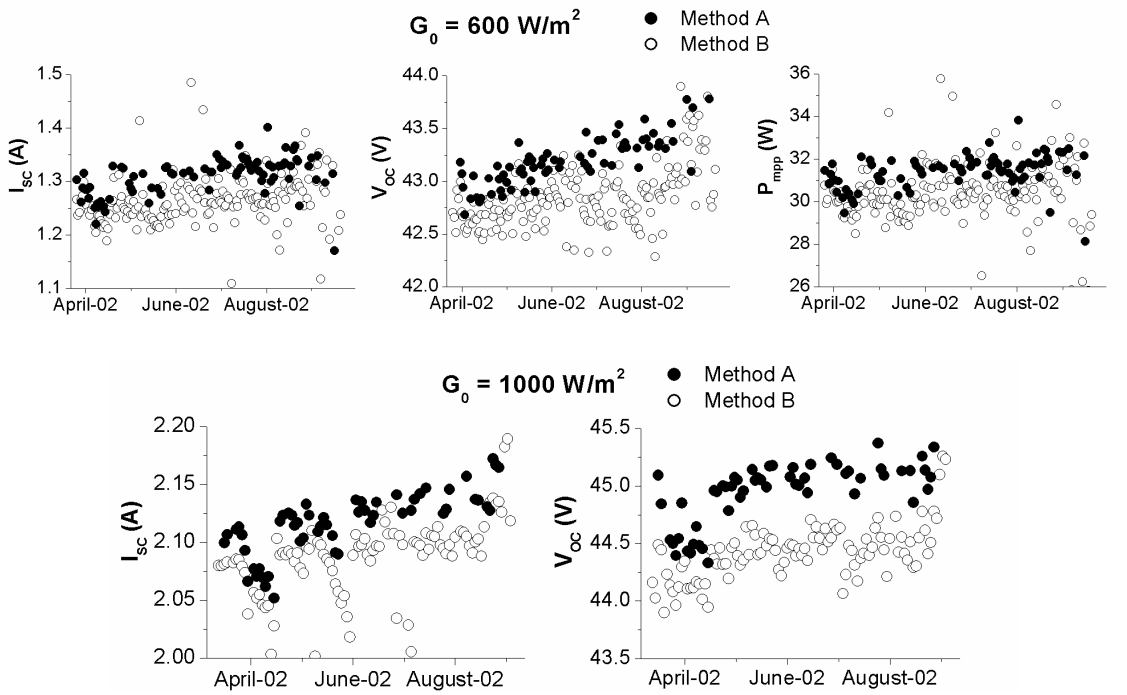

Figure 5.12: Comparison between data analysis with thorough filtering (method A) and with only basic filtering (method B) for 600 and 1000 W/m^2.

Finally, it is of interest to note that the accuracy by which field test data can be analyzed also depends on where the field test is conducted. In low-latitude climates with small seasonal variations in weather conditions the results can be analyzed with high precision. At locations like southern Finland seasonal variations are very large and the solar angle of incidence varies a lot throughout the year. This makes a detailed analysis of field data more difficult. In low-latitude climates, other filtering parameters may give better tools for improving analysis accuracy. Such parameters could include the spectral distribution of sunlight and wind speed at the module surface. If day-to-day changes in performance parameters can be analyzed with very high accuracy, it may be possible to search for correlations between daily stress (calculated, for example, from the time the module spends at high temperatures during the day or from the difference between maximum and minimum module temperatures) and daily degradation in performance parameters. This would bring photovoltaic field test research closer to answering the basic questions regarding the relevance of different stress factors in the field and in the laboratory.

5.3. Thermal stress prediction in BIPV modules

(Publication V)

Weather conditions vary a lot between different geographical locations. The conditions which PV modules should endure include all climates on Earth (for the purpose of this discussion, the usage of modules in space is disregarded). Photovoltaic modules are used in the Arctic and in the tropics. Module lifetime should therefore be predicted as a site-dependent value rather than as a constant. However, this requires an enormous amount of data on aging factors such as temperatures, humidity, irradiance and rain from around the world, as well as precise information on the dependence of module lifetime on all of these factors. This is not possible at the present level of knowledge, but temperature-driven aging can be sufficiently well modeled to permit meaningful calculations of thermal stress on modules in different locations.

Module temperature is determined primarily by plane-of-array irradiance, ambient temperature and wind speed on the module surface. These are basic meteorological parameters and they can be found or calculated from meteorological databases. As shown in Table 3.1, temperature is an important factor in all thin-film PV degradation mechanisms. As will be shown below, the temperature-dependent aging process can in many cases be modeled in a simple way. This is the starting point for the work presented in Publication V, where a model for heat transfer of a BIPV facade with a-Si modules was used to calculate temperature stress at different European locations from meteorological data. The model allows a comparison to be made between the rates of thermal degradation at these locations. This is a simple way of studying differences between climates without conducting long and expensive field tests at several locations.

5.3.1 Modeling of temperature-dependent degradation

Temperature-dependent degradation can often be theoretically modeled since many transport processes and chemical reactions include parameters with simple temperature dependencies. In the case of PV modules this is exemplified by the exponential temperature dependence of water diffusion coefficients in the encapsulant and by the reaction rate of corrosive reactions. For the latter, the rate constant k is described by the empirical Arrhenius equation

$$k(T) = C_A \cdot \exp(-E_a/k_B T), \tag{5.1}$$

where C_A is a constant, E_a is the activation energy and k_B is Boltzmann's constant. C_A and E_a can often be determined experimentally. The following presentation will focus on degradation mechanisms driven by chemical reactions at the rate given by Eq. 5.1, but it can with suitable modifications be applied also to model other exponentially temperature-dependent parameters and processes. It should be mentioned that the Eyring equation provides a slightly more versatile alternative to Eq. 5.1 and that these equations need to be applied with care in service lifetime prediction [93].

This study correlates the thermal stress which modules are exposed to in the field with the stress of an accelerated high-temperature test in the laboratory. As shown in publication V, assuming that the performance loss is directly proportional to how far the

degradation reaction has proceeded and that the reaction rate is described by Eq. 5.1, the relation between lifetime in the field, τ_N, and lifetime in the accelerated test, τ_A, becomes

$$\tau_N = \frac{\tau_A}{\sum_i \gamma_i \cdot \exp\left[E_a \left(\frac{1}{k_B T_A} - \frac{1}{k_B T_i} \right) \right]}, \tag{5.2}$$

where γ_i is the fraction of a year which the module spends at temperature T_i in the field and T_A is the temperature at which the accelerated aging test is conducted. The denominator on the right hand side is the acceleration factor, and it is evident that module temperature histograms are needed in its calculation. The work presented here focuses on the measurement and modeling of temperature histograms for the BIPV facade shown in Figure 5.3.

5.3.2 Heat transfer modeling of BIPV facade

The aim of modeling heat transfer in the BIPV facade in this work was to predict module temperature histograms from measured G and T_{amb} values. Figure 5.13 shows a schematic cross-section of the facade, with thicknesses of the various parts indicated. Heat transfer in the facade was modeled with convective, conductive and radiative transfer equations for each node indicated in Figure 5.13. Nodes 1-4 also contained a heat sink representing their heat capacity, and node 2 included the heat source of absorption of sunlight in the module. Node 0 represents the ambient environment.

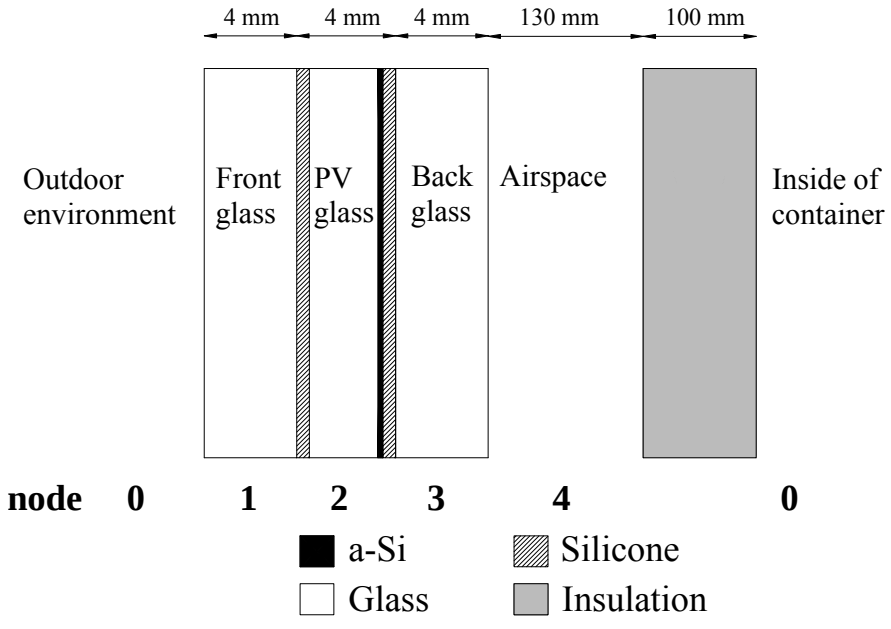

Figure 5.13: The structure of the BIPV facade.

The input parameters to the heat transfer equations were time series of G and T_{amb}. Wind speed was included as an average wind convection coefficient at node 1, not as an input parameter due to the lack of wind measurement data. For each node, a balance equation was written equalling the incoming and outgoing heat fluxes with heat sources

and sinks included. The system of equations was then solved numerically at each time to yield the time series of node temperatures. The node of particular interest was the PV glass at node 2.

5.3.3 The effect of geographical location on thermal stress

Module temperature measurements were conducted when the facade was in operation, and this information was compared to the temperatures predicted by the heat transfer model from the G and T_{amb} data measured during the same period. Figure 5.14 shows the high-temperature end of the measured and modeled yearly histograms. The width of each temperature interval in the histogram is 1°C. It can be seen that the model approximated the cumulative high temperature stress well, although it slightly underestimated the height of the curve at most points.

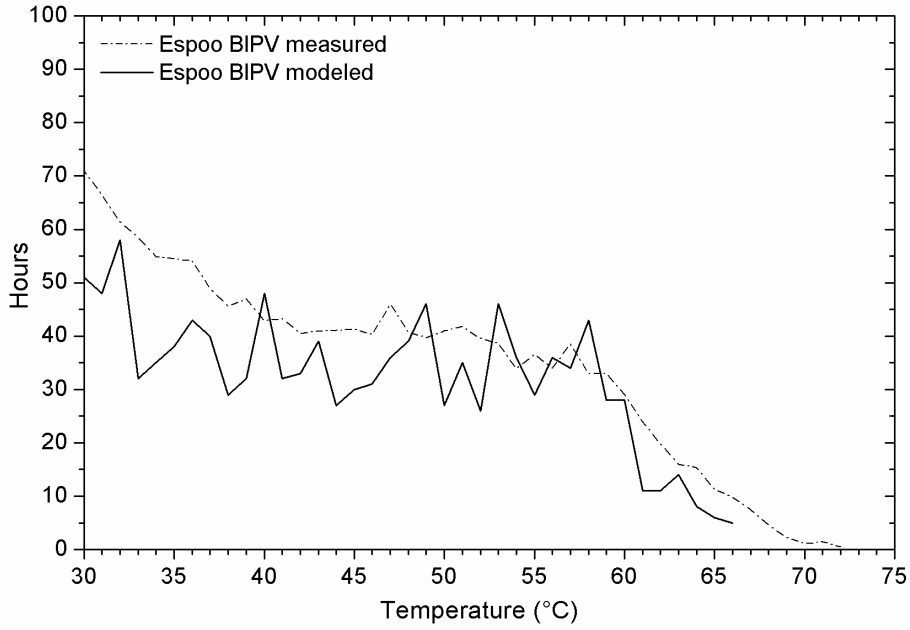

Figure 5.14: Comparison between measured and modeled yearly high-temperature histograms.

As an example in studying thermal stress at different locations, yearly meteorological data for Paris (48°48' N) and Lisbon (38°44' N) was used to calculate the histograms which the facade modules would be exposed to at those locations if they were installed in the same vertical installation which was used in Espoo. These histograms are presented in Figure 5.15, again with 1°C temperature intervals. It can be observed that the difference between the two locations was large; Lisbon had much more hours at temperatures above 30°C. To show how this translates into differences in thermal stress, the histogram data from Figure 5.15 was used to calculate the acceleration factors, determined by Eq. 5.2, for two activation energies as a function of accelerated aging temperature. The measured data in Figure 5.14 was also included, as was the yearly temperature data measured from the free standing roof-integrated a-Si facade shown in Figure 5.4.

Acceleration factors were used to calculate the accelerated aging duration needed to simulate 30 years of outdoor exposure. This duration was expressed as a function of stress temperature and plotted for each of the studied locations. The activation energies of the hypothetical degradation mechanisms were taken to be 0.4 eV and 1.0 eV. This yielded the curves shown in Figure 5.16.

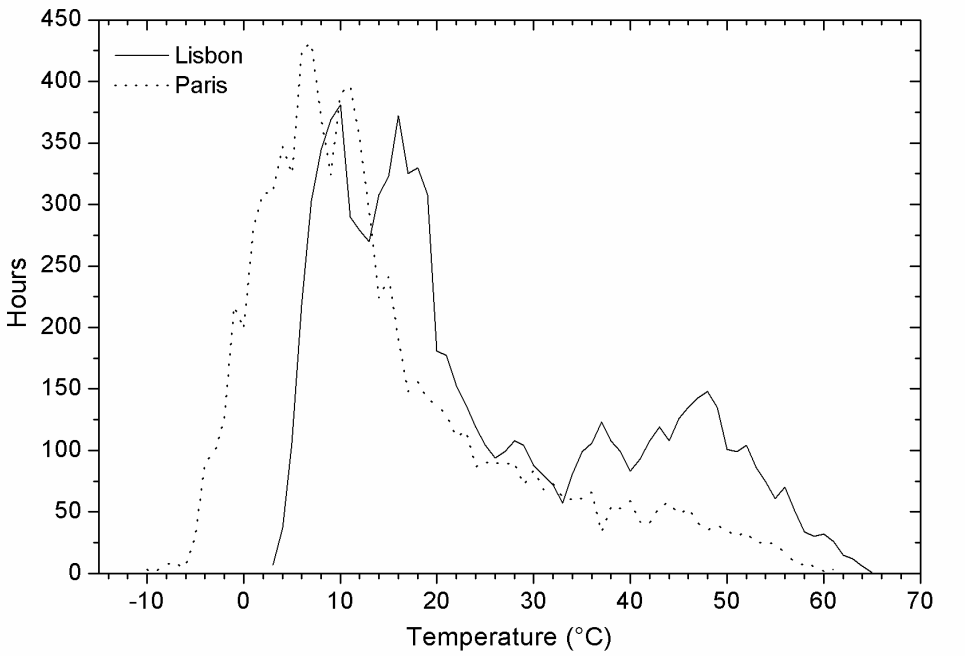

Figure 5.15: Predicted yearly temperature histograms for the studied BIPV facade if deployed at Paris, France, and Lisbon, Portugal.

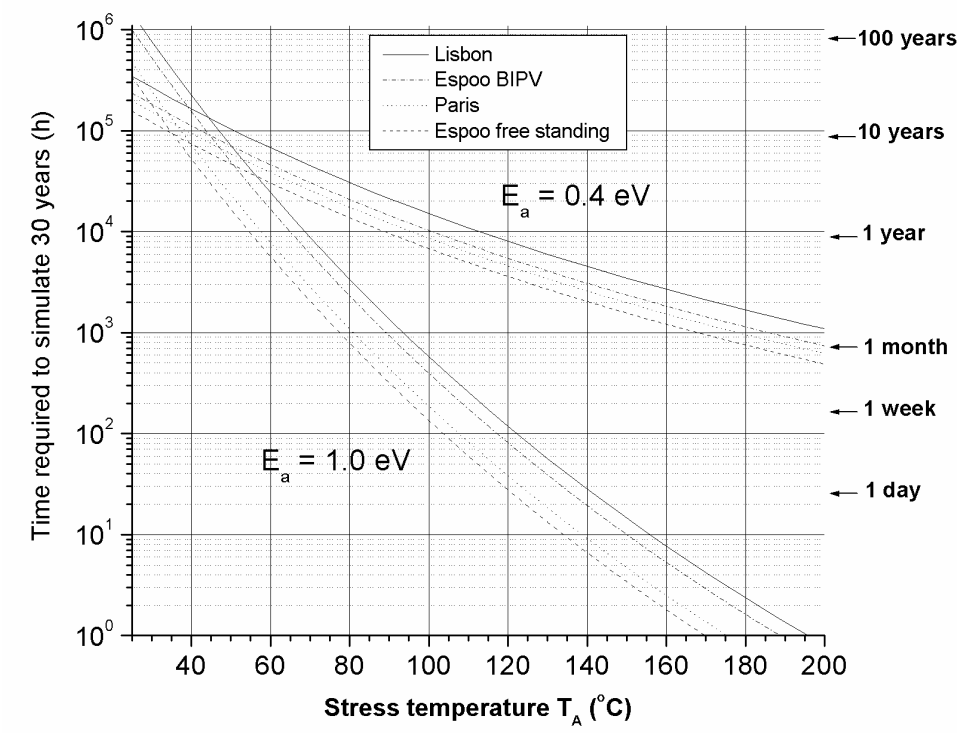

Figure 5.16: Time needed to simulate 30 years of outdoor use as a function of accelerated aging temperature.

It can be seen that the greater thermal stress in Lisbon, seen in Figure 5.15, resulted in a 50% higher accelerated stress time than in the Espoo BIPV case. The effect of the activation energy on required stress time was particularly marked in the difference between the Espoo BIPV and Paris cases. A comparison of temperature histograms shows that Espoo BIPV had higher maximum temperatures than Paris (70^{o}C compared to 60^{o}C), but Paris had more data at intermediate temperatures, 10^{o}C–30^{o}C. For 0.4 eV, the stress curves in Figure 5.16 were quite close to each other, but for 1.0 eV the high temperature data was crucial and the Paris curve therefore lay significantly below the Espoo BIPV curve. This exemplifies how the temperature histogram and the activation energy together determine the degradation caused by thermal stress. It can also be noted that the tilt angle of PV modules plays a role in determining their temperature histograms. The reason why higher temperatures were achieved in Espoo than in Paris was probably that the incidence angle of sunlight on the vertical facade was smaller in Espoo in the summer.

6. Concluding remarks

Improvements in the operating lifetime of PV modules reduce the price of photovoltaic electricity. Many lifetime and stability questions have to date been studied to a limited degree. Prospects for improving the competitiveness of PV electricity in the near future through stability improvements are therefore promising. PV module stability depends on the temperature-, UV- and moisture stability of the cell materials and the interconnects. Protection from the exterior environment is also crucial. Lifetime research therefore ideally requires multidisciplinary approaches which combine expertise in solid state physics, polymer science, corrosion science, electrochemistry, microscopy, field testing, accelerated aging and statistical mathematics. The scientific challenges are significant, but so is the potential payoff.

This thesis is an investigation into new methods for evaluating and predicting the stability of thin-film PV modules and their encapsulants. Ensuring that thin-film modules have a sufficiently long lifetime is important if the cost benefits of thin-film photovoltaics are to be fully utilized. The primary stability challenge for thin-film PV technology will most likely be how sufficiently long module lifetimes can be ensured without increasing costs too much. Accurate stability diagnostics are therefore essential in lifetime testing of thin-film PV modules. The importance of two areas of lifetime research is emphasized in the diagnostic methods developed in this thesis: the study of water penetration through module encapsulants and the identification of degradation mechanisms in field tests.

The development of a moisture sensor of micrometer thickness for the study of water penetration into glass/polymer laminates is described in this thesis. The primary benefits of this method compared to alternative moisture tests for PV modules or glass/polymer laminates are that the measurement does not affect the process under study and that the amount of water which has penetrated the film can be evaluated. With the electrode geometry used in this thesis, a measurable signal was obtained when approximately 10 μg of water had penetrated the TiO_2 film. Sensor response was linear for sensors open to the environment and for encapsulated sensors. The concept developed for moisture measurement in encapsulated structures in this thesis can be extended and improved in a number of ways. In addition to PV module testing, it can also be applied to encapsulation testing for microelectronic devices.

The moisture sensor was applied in this thesis to a measurement of water absorption and desorption rates from glass/EVA/glass laminates. Water desorption from a sample at 50^{o}C temperature to room temperature surroundings was found to be approximately 16 times as fast as water absorption at room temperature. Even a sample temperature of 35^{o}C resulted in desorption which was 4 times faster than ambient absorption. Results indicate that unframed, EVA-encapsulated PV modules probably dry out significantly in the summer since temperatures above 50^{o}C are very common in sunny conditions. The moisture-limited lifetime of PV modules is difficult to model, but absorption and desorption studies in field tests and in the laboratory will be crucial when theoretical understanding is sought in this area of lifetime research. The moisture sensor concept developed in this thesis should be applicable also in outdoor tests as long as sensor stability can be ensured.

The field test research in this thesis includes identification of degradation mechanisms in field-tested modules through small-sample analysis. In a study of CdTe modules, the results pointed to two separate degradation mechanisms which lowered the fill factor of the modules: an increase in TCO resistance and a widening of the depletion region through dopant transportation away from the junction. It is suggested that small-sample analysis is a valuable tool especially for analyzing fill factor degradation, whereas I_{SC} or V_{OC} degradation is more difficult to analyze accurately without greatly increasing the number of samples taken from each module.

This thesis also focuses on the development of a data filtering methodology for improving the accuracy of field data analysis. The data collected in field test measurements always has to be filtered in some way, and the analytics developed in this thesis allow quantitative comparisons between different filtering options. In the example presented for CIGS modules, detailed filtering reduced the residual variance in V_{OC} data by 73% at 600 W/m^2 and by 40% at 1000 W/m^2 compared to variances obtained with a standard analysis method. Residual variance in I_{SC} data was reduced by 61% at 600 W/m^2 and 79% at 1000 W/m^2. If more meteorological and module variables can be measured with high accuracy in the future, the method developed here may eventually make it possible to correlate the occurrence of a given outdoor stress factor with a consequent degradation in module performance.

This thesis also includes work on thermal modeling of thin-film BIPV facades for estimating the thermal stress which the modules are exposed to. It was demonstrated that a simple heat-transfer model of the facade predicts the temperature histograms of the modules from measured meteorological variables with reasonable accuracy. The model was used to calculate that the yearly stress on modules in this facade would be approximately 50% higher in Lisbon, Portugal than in Espoo, Finland, meaning that an accelerated thermal test simulating the conditions in Lisbon should be 50% longer than a test simulating the conditions in Espoo. More precise lifetime modeling for different climates would require that other outdoor stress factors are included in the analysis. Extending the analysis to factors such as temperature cycles or moisture exposure will be a challenging task in the future.

References

[1] World Population Prospects, The 2004 Revision. ESA/P/WP.193 United Nations, New York 2005. www.un.org

[2] World Energy Outlook 2005. International Energy Agency 2005. www.iea.org

[3] N.Myers. Lifting the veil on perverse subsidies. *Nature* **392** (1998), p.327-328.

[4] TRENDS IN PHOTOVOLTAIC APPLICATIONS, Report IEA-PVPS T1-14:2005.
www.iea-pvps.org

[5] EPIA Roadmap, European Photovoltaic Industry Association, 2004.
www.epia.org

[6] A.Czanderna, G.Jorgensen. Accelerated life testing and service lifetime prediction for PV technologies in the twenty-first century. *Electrochemical Society Proceedings 99-11 (Photovoltaics for the 21st century)* 1999, 57-67.

[7] T.McMahon. Accelerated Testing and Failure of Thin-Film PV Modules. *Progress in Photovoltaics* **12** (2004), p.235-248.

[8] Handbook of Photovoltaic Science and Engineering. John Wiley & Sons 2003.

[9] C.Mathers. Upper limit of efficiency for photovoltaic cells. *Journal of Applied Physics* **48** (1977), p.3181-3182.

[10] M.Green, K.Emery, D.King, S.Igari, W.Warta. Solar Cell Efficiency Tables (Version 26). *Progress in Photovoltaics* **13** (2005), p.387-392.

[11] J.Werner, presentation at the Nordic Workshop on Solar Electricity, Copenhagen 28.4.2004.

[12] K.Chopra, P.Paulson, V.Dutta. Thin-Film Solar Cells: An Overview. *Progress in Photovoltaics* **12** (2004), p.69-92.

[13] G.Mon, L.Wen, R.Ross. Water-module interaction studies. *Conference Record of the 20th IEEE PV Specialists Conference*, 1988, p.1098-1102.

[14] IEC International Standard 1215: Crystalline silicon terrestrial photovoltaic (PV) modules – Design qualification and type approval. Geneva, Switzerland, 1993.

[15] IEC International Standard 1646: Thin-film terrestrial photovoltaic (PV) modules – Design qualification and type approval. Geneva, Switzerland, 1996.

[16] IEEE Standard 1262-1995: Recommended Practice for Qualification of Photovoltaic (PV) Modules. IEEE, 1996.

[17] S.Roschier. Development of Procedures for Performance Measurements and Lifetime Testing of Thin Film Photovoltaic Devices. Doctoral Dissertation, Helsinki University of Technology 2002.

[18] K.Dobson, I.Visoly-Fisher, G.Hodes, D.Cahen. Stability of CdTe-CdS thin-film solar cells. *Solar Energy Materials & Solar Cells* **62** (2000), p.295-325.

[19] I.Visoly-Fisher, K.Dobson, J.Nair, E.Bezalel, G.Hodes, D.Cahen. Factors Affecting the Stability of CdTe/CdS Solar Cells Deduced from Stress Tests at Elevated Temperature. *Advanced Materials* **13** (2003), p.289-299.

[20] S.Hegedus, B.McCandless, R.Birkmire. Analysis of Stress-Induced Degradation in CdS/CdTe Solar Cells. *Conference Record of the 28th IEEE PV Specialists Conference*, 2000, p.535-538.

[21] J.Hiltner, J.Sites. Stability of CdTe Solar Cells at Elevated Temperatures: Bias, Temperature and Cu Dependence. *AIP Conference Proceedings* **462** (1999), p.170-175.

[22] Powell R, Sasala R, Rich G, Steele M, Bihn K, Reiter N, Cox S, Dorer G. Stability testing of CdTe/CdS thin-film photovoltaic modules. *Conference Record of the 25th IEEE PV Specialists Conference*, 1996, p.785-788.

[23] P.Meyers, S.Asher, M.Al-Jassim. A Search for Degradation Mechanisms of CdTe/CdS Solar Cells. *Materials Research Society Symposium Proceedings* **426** (1996), p.317-324.

[24] K.Dobson, I.Visoly-Fisher, G.Hodes, D.Cahen. Stabilizing CdTe/CdS Solar Cells with Cu-Containing Contacts to p-CdTe. *Advanced Materials* **13** (2001), p.1495-1499.

[25] N.Romeo, A.Bosio, R.Tedeschi, V.Canevari. Back contacts to CSS CdS/CdTe solar cells and stability of performances. *Thin Solid Films* **361-362** (2000), p.327-329.

[26] S.Degrave, P.Nollet, G.Stojanoska, M.Burgelman, K.Durose. Interpretation of Ageing Experiments on CdTe/CdS Solar Cells. *Proceedings of the 17th European PVSEC*, 2001, p.1058-1061.

[27] T.McMahon, T.Berniard, D.Albin. Nonlinear shunt paths in thin-film CdTe solar cells. *Journal of Applied Physics* **97** (2005), p.54053-1–54053-5.

[28] J.-F.Guillemoles, U.Rau, L.Kronik, H.-W.Schock, D.Cahen. Cu(In,Ga)Se_2 Solar Cells: Device Stability Based on Chemical Flexibility. *Advanced Materials* **11** (1999), p.957-961.

[29] J.-F.Guillemoles, L.Kronik, D.Cahen, U.Rau, A.Jasenek, H.-W.Schock. Stability Issues of Cu(In,Ga)Se_2-Based Solar Cells. *Journal of Physical Chemistry B* **104** (2000), p.4849-4862.

[30] J.-F.Guillemoles. Stability of Cu(In,Ga)Se_2 solar cells: a thermodynamic approach. *Thin Solid Films* **361-362** (2000), p.338-345.

[31] J.-F.Guillemoles. The puzzle of Cu(In,Ga)Se_2 (CIGS) solar cell stability. *Thin Solid Films* **403-404** (2002), p.405-409.

[32] M.Schmidt, D.Braunger, R.Schäffler, H.W.Schock, U.Rau. Influence of damp heat on the electrical properties of Cu(In,Ga)Se_2 solar cells. *Thin Solid Films* **361-362** (2000), p.283-287.

[33] M.Igalson, M.Wimbor, J.Wennerberg. The change of the electronic properties of CIGS devices induced by the 'damp heat' treatment. *Thin Solid Films* **403-404** (2002), p.320-324.

[34] C.Deibel, V.Dyakonov, J.Parisi, J.Palm, S.Zweigart, F.Karg. Influence of damp heat testing on the electrical characteristics of Cu(In,Ga)$(S,Se)_2$ solar cells. *Thin Solid Films* **403-404** (2002), p.325-330.

[35] C.Heske, U.Groh, L.Weinhardt, O.Fuchs, B.Holder, E.Umbach, C.Bostedt, L.Terminello, S.Zweigart, T.Niesen, F.Karg. Damp-heat induced sulfate formation in Cu(In,Ga)$(S,Se)_2$-based thin-film solar cells. *Applied Physics Letters*, 2002, p.4550-4552

[36] C.Heske, U.Groh, O.Fuchs, L.Weinhardt, E.Umbach, T.Schedel-Niedrig, C.Fischer, M.Lux-Steiner, S.Zweigart, T.Niesen, F.Karg, J.Denlinger, B.Rude, C.Andrus, F.Powell. Monitoring chemical reactions at a liquid-solid interface: Water on CuIn$(S,Se)_2$ thin film solar cell absorbers. *Journal of Chemical Physics* **119** (2003), p.10467-10470.

[37] J.Malmström, J.Wennerberg, L.Stolt. A study of the influence of the Ga content on the long term stability of Cu(In,Ga)Se_2 thin film solar cells. *Thin Solid Films* **431-432** (2003), p.436-442.

[38] G.Medvedkin, E.Terukov, Y.Hasegawa, K.Hirose, K.Sato. Microdefects and point defects optically detected in Cu(In,Ga)Se_2 thin film solar cells exposed to the damp and heating. *Solar Energy Materials & Solar Cells* **75** (2003), p.127-133.

[39] D.Redfield, R.Bube. Evaluation of Degradation in Amorphous Silicon Solar Cells. *Conference Record of the 21st IEEE PV Specialists Conference*, 1990, p.1506-1509.

[40] C.Wronski. Amorphous Silicon Photovoltaics: Order From Disorder. *Conference Record of the 28th IEEE PV Specialists Conference*, 2000, p.1-6.

[41] B.Samanta, D.Das, A.Barua. Role of buffer layer at the p/i interface on the stabilized efficiency of a-Si solar cells. *Solar Energy Materials & Solar Cells* **46** (1997), p.233-237

[42] J.Lathrop, P.Williamson. Failure mechanisms in amorphous silicon solar cells. *Conference Record of the 19th IEEE PV Specialists Conference*, 1987, p.200-203.

[43] T.McMahon, M.Bennett. Metastable shunt paths in a-Si solar cells. *Solar Energy Materials & Solar Cells* **41/42** (1996), p.465-473.

[44] V.Singh, O.Erickson, J.Chao. Analysis of contact degradation at the CdTe-electrode interface in thin film CdTe-CdS solar cells. *Journal of Applied Physics* **78** (1995), p.4538-4542.

[45] D.Bätzner, A.Romeo, H.Zogg, R.Wendt, A.Tiwari. Development of efficient and stable back contacts on CdTe/CdS solar cells. *Thin Solid Films* **387** (2001), p.151-154.

[46] D.Bätzner, A.Romeo, M.Terheggen, M.Döbeli, H.Zogg, A.Tiwari. Stability aspects in CdTe/CdS solar cells. *Thin Solid Films* **451-452** (2004), p.536-543.

[47] W.Shafarman, J.Phillips. Current-voltage characterization of $CuInSe_2$/CdS solar cells deposited by different methods. *Conference Record of the 23rd IEEE PV Specialists Conference*, 1993, p.453-458.

[48] W.Shafarman, J.Phillips. Direct current-voltage measurements of the Mo/$CuInSe_2$ contact on operating solar cells. *Conference Record of the 25th IEEE PV Specialists Conference*, 1996, p.917-919.

[49] D.Carlson, R.Romero, F.Willing, D.Meakin, L.Gonzalez, R.Murphy, H.Moutinho, M.Al-Jassim. Corrosion Effects in Thin-Film Photovoltaic Modules. *Progress in Photovoltaics* **11** (2003), p.377-386.

[50] C.Osterwald, T.McMahon, J.del Cueto. Electrochemical corrosion of SnO_2:F transparent conducting layers in thin-film photovoltaic modules. *Solar Energy Materials & Solar Cells* **79** (2003), p.21-33.

[51] G.Mon, J.Orehotsky, R.Ross, G.Whitla. Predicting Electrochemical Breakdown in Terrestrial Photovoltaic Modules. *Conference Record of the 17th IEEE PV Specialists Conference*, 1984, p.682-692.

[52] G.Mon, G.Whitla, R.Ross, M.Neff. The Role of Electrical Insulation Systems in Electrochemical Degradation of Terrestrial Photovoltaic Modules. *IEEE Transactions on Electrical Insulation* EI-20 (1985), p.989-995.

[53] G.Mon, L.Wen, J.Meyer, R.Ross. Electrochemical and galvanic corrosion effects in thin-film photovoltaic modules. *Conference Record of the 20th IEEE PV Specialists Conference*, 1988, p.108-113.

[54] G.Mon, L.Wen, R.Ross, D.Adent. Effects of Temperature and Moisture on Module Leakage Currents. *Conference Record of the 18th IEEE PV Specialists Conference*, 1984, p.1179.

[55] J.Wennerberg, J.Kessler, M.Bodegård, L.Stolt. Damp-heat testing of high performance CIGS thin-film solar cells. *Proceedings of the 2nd World Conference on Photovoltaic Solar Energy Conversion*, 1998, p.1161-1164

[56] J.Wennerberg, J.Kessler, L.Stolt. Degradation mechanisms of Cu(In,Ga)Se_2 Thin Film PV Modules. *Proceedings of the 16th European Photovoltaic Solar Energy Conference,* 2000, p.309-312.

[57] J.Wennerberg, J.Kessler, L.Stolt. Cu(In,Ga)Se_2-based thin-film photovoltaic modules optimized for long-term performance. *Solar Energy Materials & Solar Cells* **75** (2003), p.47-55.

[58] J.Klaer, R.Klenk, A.Boden, A.Neisser, C.Kaufmann, R.Scheer, H.-W.Schock. Damp Heat Stability of Chalcopyrite Mini-Modules: Evaluation of Specific Test Structures. *Conference Record of the 31st IEEE PV Specialists Conference*, 2005, p.336-339.

[59] L.Wen, G.Mon, E.Jetter, R.Ross. Electromigration in thin-film photovoltaic module metallization systems. *Conference Record of the 20th IEEE PV Specialists Conference*, 1988, p.364-369.

[60] R.Ross, G.Mon, L.Wen, R.Sugimura. Measurement and Characterization of Voltage- and Current-Induced Degradation of Thin-Film Photovoltaic Modules. *Solar Cells* **27** (1989), p.298-298.

[61] G.Jorgensen, K.Terwilliger, S.Glick, J.Pern, T.McMahon. Materials Testing for PV Module Encapsulation. NREL/CP-520-33578 (2003).

[62] G.Jorgensen, K.Terwilliger, M.Kempe, T.McMahon. Testing of Packaging Materials for Improved PV Module reliability. *Conference Record of the 31st IEEE PV Specialists Conference*, 2005, p.499-502.

[63] A.Czanderna, F.Pern. Encapsulation of PV modules using ethylene vinyl acetate copolymer as a pottant: A critical review. *Solar Energy Materials & Solar Cells* **43** (1996), p.101-181.

[64] T.Kojima, T.Yanagisawa. The evaluation of accelerated test for degradation of a stacked a-Si solar cell and EVA films. *Solar Energy Materials & Solar Cells* **81** (2004), p.119-123.

[65] N.Allen, M.Edge, M.Rodriguez, C.Liauw, E.Fontan. Aspects of the thermal oxidation, yellowing and stabilisation of ethylene vinyl acetate copolymer. *Polymer Degradation and Stability* **71** (2001), p.1-14.

[66] F.Pern, S.Glick. Photothermal stability of encapsulated Si solar cells and encapsulation materials upon accelerated exposures. *Solar Energy Materials & Solar Cells* **61** (2000), p.153-188.

[67] M.Kempe. Control of Moisture Ingress into Photovoltaic Modules. *Conference Record of the 31st IEEE PV Specialists Conference*, 2005, p.503-506.

[68] M.Hahn, W.Berry, L.Mrig. Comparative Short Term / Long Term Field Test Performance and Stability of Tandem and Single Junction a-Si Modules. *Conference Record of the 21st IEEE PV Specialists Conference*, 1990, p.1057-1061.

[69] J.del Cueto, T.McMahon. Performance of Single-Junction a-Si Modules Under Varying Conditions in the Field. *Conference Record of the 26th IEEE PV Specialists Conference*, 2000, p.1205-1208.

[70] K.Akhmad, A.Kitamura, F.Yamamoto, H.Okamoto, H.Takakura, Y.Hamakawa. Outdoor performance of amorphous silicon and polycrystalline silicon PV modules. *Solar Energy Materials & Solar Cells* **46** (1997), p.209-218.

[71] J.del Cueto. Review of the Field Performance of One Cadmium Telluride Module. *Progress in Photovoltaics* **6** (1998), p.433-446.

[72] H.Ullal, K.Zweibel, B.von Roedem. Current Status of Polycrystalline Thin-Film PV Technologies. *Conference Record of the 26th IEEE PV Specialists Conference*, 1997, p.301-305.

[73] J.del Cueto, T.McMahon. Analysis of Leakage Currents in Photovoltaic Modules under High-Voltage Bias in the Field. *Progress in Photovoltaics* **10** (2002), p.15-28.

[74] T.McMahon, T.Basso, S.Rummel. Cell Shunt Resistance and Photovoltaic Module Performance. *Conference Record of the 25th IEEE PV Specialists Conference*, 1996, p.1291-1294.

[75] E.Meyer, E.van Dyk. Characterization of degradation in thin-film photovoltaic module performance parameters. *Renewable Energy* **28** (2003), p.1455-1469.

[76] E.Meyer, E.van Dyk. Analysis of degradation in $CuInSe_2$ photovoltaic modules. *Physica Status Solidi* **201** (2004), p.2245-2250.

[77] S.Spiering, D.Hariskos, S.Schröder, M.Powalla. Stability behaviour of Cd-free $Cu(In,Ga)Se_2$ solar modules with In_2S_3 buffer layer prepared by atomic layer deposition. *Thin Solid Films* **480-481** (2005), p.195-198.

[78] C.Lund, K.Luczak, T.Pryor, J.Cornish, P.Jennings, P.Knipe, F.Ahjum. Field and laboratory studies of the stability of amorphous silicon solar cells and modules. *Renewable Energy* **22** (2001), p.287-294.

[79] N.Dhere, H.Patil, S.Bet, A.Pai, V.Hadagali, U.Avachat. Investigation of Degradation Aspects of Field Deployed Photovoltaic Modules. NREL/CD-520-33586 (2003), p.958-961

[80] P.Klemchuk, M.Ezrin, G.Lavigne, W.Holley, J.Galica, S.Agro. Investigation of the degradation and stabilization of EVA-based encapsulant in field-aged solar energy modules. *Polymer Degradation and Stability* **55** (1997), p.347-365.

[81] A.Gxasheka, E.van Dyk, E.Meyer. Evaluation of performance parameters of PV modules deployed outdoors. *Renewable Energy* **30** (2005), p.611-620.

[82] E.van Dyk, J.Chamel, A.Gxasheka. Investigation of delamination in an edge-defined filmd-fed growth photovoltaic module. *Solar Energy Materials & Solar Cells* **88** (2005), p.403-411.

[83] D.Burch, J.Martin, M.VanLandingham. Computer Analysis of a Polymer Coating Exposed to Field Weather Conditions. *Journal of Coatings Technology* **74** (2002), p.75-86.

[84] E.Traversa, G.Gnappi, A.Montenero, G.Gusmano. Ceramic thin films by sol-gel processing as novel materials for integrated humidity sensors, *Sensors and Actuators B* **31** (1996), p.59-70.

[85] W.-P.Tai, J.-H.Oh. Preparation and humidity sensing behaviors of nanocrystalline bilayered SnO_2/TiO_2 films. *Thin Solid Films* **422** (2002), p.220-224.

[86] Y.-C.Yeh, T.-Y.Tseng, D.-A.Chang, Electrical properties of porous titania ceramic humidity sensors, *Journal of the American Ceramic Society* **72** (1989) 1472-1475.

[87] G. Huyberechts, L. Frisson. In-situ formation of humidity-sensitive devices for the evaluation of solar panel encapsulations. *Sensors and Actuators B* **26-27** (1995), p.308-311.

[88] J. Crank, *Mathematics of diffusion*, Oxford University Press, London, 1st edn., 1950, p. 45.

[89] E.Traversa. Ceramic sensors for humidity detection: the state-of-the-art and future developments. *Sensors and Actuators B* **23** (1995), p.135-156.

[90] S.Marais, Y.Hirata, D.Langevin, C.Chappey, T.Nguyen, M.Metayer. Permeation and Sorption of Water and Gases Through EVA Copolymers Films. *Materials Research Innovations* **6** (2002), p. 79-88.

[91] T.Carlsson. Experimental setup for full scale field tests of CdTe and CIS thin-film photovoltaic modules. Master's Thesis, Helsinki University of Technology 2001.

[92] P.Lund, E.Vartiainen, M.Ross, K.Mäki-Petäys, J.Leppänen, A.-G.Hestnes, I.Andersen, A.Lien, O.Skarstein, K.Morcant, D.Guillardeu, W.Jager. EU-JOULE JOR3-CT96-0096 ASICOM Amorphous-Si Photovoltaics for Commercial Buildings, *Final Report to the European Commission, Summary*: Helsinki University of Technology, Advanced Energy Systems 1999.

[93] K.Gillen, M.Celina, R.Clough, J.Wise. Extrapolation of accelerated aging data – Arrhenius or erroneous? *Trends in Polymer Science* **5** (1997), p.250-257.

ISBN 951-22-8274-7
ISBN 951-22-8275-5 (PDF)
ISSN 1795-2239
ISSN 1795-4584 (PDF)